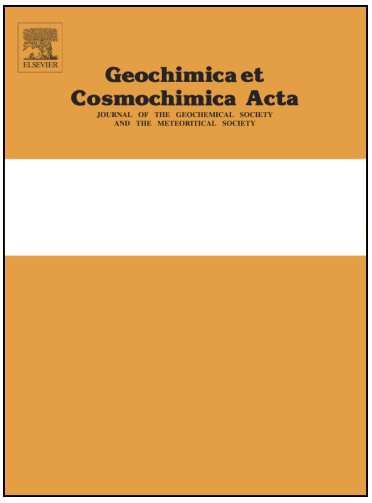

Identifying thermogenic and microbial methane in deep water Gulf of Mexico Reservoirs

Nivedita Thiagarajan, Nami Kitchen, Hao Xie, Camilo Ponton, Michael Lawson, Michael Formolo, John Eiler

PII: S0016-7037(20)30126-5
DOI: https://doi.org/10.1016/j.gca.2020.02.016
Reference: GCA 11655

To appear in: *Geochimica et Cosmochimica Acta*

Received Date: 6 August 2018
Accepted Date: 14 February 2020

Please cite this article as: Thiagarajan, N., Kitchen, N., Xie, H., Ponton, C., Lawson, M., Formolo, M., Eiler, J., Identifying thermogenic and microbial methane in deep water Gulf of Mexico Reservoirs, *Geochimica et Cosmochimica Acta* (2020), doi: https://doi.org/10.1016/j.gca.2020.02.016

Identifying thermogenic and microbial methane in deep water Gulf of Mexico Reservoirs

Nivedita Thiagarajan[1], Nami Kitchen[1], Hao Xie[1], Camilo Ponton[1], Michael Lawson[2], Michael Formolo[3], John Eiler[1] (in prep for GCA)

[1]*Department of Geological and Planetary Sciences. California Institute of Technology Pasadena, CA 91125*

[2]*ExxonMobil Upstream Business Development, Spring, TX 77389*

[3]*ExxonMobil Upstream Research Company, Spring, TX 77389*

ABSTRACT

The Gulf of Mexico (GOM) produces 5% of total U.S. dry gas production (USEIA, 2016). Despite this, the proportion of microbial and thermogenic methane in discovered and producing fields from this area is still not well understood. Understanding the relative contributions of these sources in subsurface environments is important to understanding how and where economically substantial amounts of methane form. In addition, this information will help identify sources of environmental emissions of hydrocarbons to the atmosphere. We apply stable isotopes including methane clumped-isotope measurements to solution and associated gases from several producing fields in the U.S. Gulf of Mexico to estimate the proportions, properties and origins of microbial and thermogenic endmembers. Clumped isotopes of methane are unique indicators of whether methane is at thermodynamic isotopic equilibrium or affected by kinetic processes. The clumped methane thermometer can provide insights into formation temperatures and/or into kinetic processes such as microbial methanogenesis, early catagenetic processes, mixing, combinatorial processes, and diffusion. In this data set, we find that some fluids have clumped isotope methane apparent temperatures consistent with the methane component being produced solely by the thermogenic breakdown of larger organic molecules at substantially greater temperatures than those reached in shallow reservoirs. A portion of these reservoirs with hot clumped isotope methane temperatures are consistent with exhibiting a kinetic isotope effect. Other reservoirs have clumped isotope methane apparent temperatures, and other isotopic and molecular proportions, consistent with mixtures of microbial and thermogenic methane. We show that in certain cases the evidence is most consistent with formation of the microbial methane in the current reservoir. However, in other cases the methane is produced at significantly shallower depths and is then transported to greater depths as a result of post generation burial of methane bearing sedimentary sequences to the current reservoir conditions. For the first time, we show that methane of an unambiguously purely microbial origin (i.e. those

that do not contain obvious contributions of thermogenic methane) is dominantly generated at temperatures less than 60°C, despite burial to greater depths. This finding suggests that, while microorganisms are able to generate methane at temperatures up to 105°C under laboratory conditions (Brock, 1985), in the Gulf of Mexico, microbial methane is dominantly produced in the 20 - 60°C window.

1. INTRODUCTION

Methane, CH_4, from microbial or thermogenic sources, is an environmentally significant greenhouse gas and an economically important natural resource. Understanding the source of methane is important in determining the origin of environmental emissions and in the exploration of natural gas. One of the main complications in understanding the origin of methane is that it can be created from a variety of mechanisms and frequently occurs as mixtures of gas from two or more sources, further complicating geochemical signatures for its origins. It has been long known that there are two microbial sources to methane (primary and secondary) and that maturation of organic matter can lead to the production of thermogenic methane. Primary microbial methane is produced from the breakdown of immature organic matter (Rice, 1981) while secondary microbial methane is produced from the microbial degradation of oils (Milkov, 2011; Milkov and Dzou, 2007). In contrast, thermogenic methane is generated during the thermal break down of larger organic molecules (Schoell, 1980; Rice, 1981; Whiticar, 1994; Hunt, 1995)).

Hydrogen and carbon isotope measurements, as well as gas molecular compositional analyses, have been widely applied to constrain the sources of methane. These signatures have established capabilities for discriminating end-member thermogenic and microbial methane, but in some cases they are ambiguous or misleading. Some gases can appear thermogenic with respect to one index and microbial with respect to another, for instance as seen in the Michigan Basin (Martini et al., 1996). Additionally, the endmember compositions assigned to microbial and thermogenic gases encompass wide ranges and overlap one another, meaning many gases could be assigned to more than one process, and it is often unclear how to quantify relative contributions of two or three sources to a mixed gas (Schoell, 1980; Whiticar, 1999).

Methane clumped isotope geochemistry provides an opportunity to improve our interpretations on the origin of methane (D. A. Stolper et al., 2014; Ono et al., 2014). Currently, these applications measure the abundance of doubly substituted isotopologues of methane ($^{13}CH_3D$ and $^{12}CH_2D_2$). The proportions of these clumped isotopologues relative to the unsubstituted (e.g. $^{12}CH_4$) and singly substituted isotopologues of the same molecule (e.g. $^{13}CH_4$, $^{12}CH_3D$) are solely a function of temperature in compounds that have reached equilibrium with respect to their distributions of isotopes among all possible isotopologues (generally described through equilibrium constants for the homogenous isotope exchange reactions) (Wang et al., 2004). Some early work measured both clumped signatures in the methane molecule together and reported them relative to the unsubstituted isotopogue (Stolper et al., 2014; Stolper et al., 2015; Douglas et al., 2016; Douglas et al., 2017; Stolper et al., 2017; Shuai et al., 2018a; Shuai et al., 2018b). However technological developments have recently allowed both clumped isotopologues to be individally measured (Young et al., 2017; Giunta et al 2019, this study).

Initial work on the characterization of thermogenic and microbial methane from a range of natural environments indicated that clumped methane isotopologues could be used to determine formation or re-equilibration temperatures of methane (Stolper et al., 2014; Inagaki et

al., 2015). Later, kinetic isotope effects in clumped isotopologues were noted both in microbial and thermogenic systems (Wang et al., 2015; Young et al., 2017; Douglas et al., 2017; Shuai et al., 2018a; Gruen et al., 2018; Ash et al., 2019; Giunta et al., 2019). Laboratory cultured methanogens and microbial methane from certain natural environments have been reported to have a kinetic isotope effect (KIE) (Wang et al., 2015; Stolper et al., 2015; Young et al., 2017; Gruen et al., 2018; Giunta et al., 2019). These KIEs tend to be correlated with hydrogen isotope disequilibrium between methane and water (in the direction of strong D depletion in product methane) and have been interpreted to be a result of a low degree of reversibility in the enzymatic reactions that allow methanogens to produce methane (Wang et al., 2015; Stolper et al., 2015), or as an artifact due to residues of anaerobic oxidation of methane (Giunta et al., 2019).

In two thermogenic gas systems, the Eagle Ford Shale and Bakken Shale, clumped isotope disequilibrium signatures have been observed (Douglas et al., 2017; Stolper et al., 2017). These reservoirs are unconventional associated gas reservoirs with clumped isotope temperatures as high as 380°C, exceeding the value expected for oil stability. These unequilibrated gases all have unusually low D/H ratios and $^{13}C/^{12}C$ ratios consistent with gases of moderate thermal maturity. These clumped isotope disequilibra signature have been interpreted to reflect a kinetic isotope effect associated with methane generation, possibly due to secondary cracking of components of the associated fluids. Evidence in favor of this idea comes from recent pyrolysis experiments on coal and shale (Shuai et al 2018) that showed that clumped isotope disequilibrium effects can be expressed during methane generation and these effects coincide with the onset of ethane cracking. The exact mechanism by which these pyrolysis experiments relate to natural thermogenic samples was not known at the time the Shuai et al. study was published, but subsequent study of the $\Delta^{13}CH_3D$ and $\Delta^{12}CH_2D_2$ anomalies of methane produced by laboratory alkane 'cracking' (Dong et al., 2019) and found in unconventional associated gases (Xie et al., 2019) indicate the primary cause is a combinatorial isotope effect associated with combination of a relatively high D/H methyl pool and a relatively low D/H abstracted or radical hydrogen atom pool. In any case, these studies show that thermogenic methane generation can be associated with kinetic isotope effects (though these may be erased by subsequent isotopic exchange).

Thus, the clumped isotope compositions of methane from natural gas may reflect multiple biological geochemical and geologic processes, including: temperatures of formation or re-equilibrating processes; kinetic isotope effects; combinatorial isotope effects; mixing; inheritance of the clumped isotope composition from a precursor such as a methyl group; and possibly mass transfer and phase separation processes such as gas expulsion (though these have not been shown to dominate clumped isotope variations in natural gases) (Douglas et al., 2017).

The U.S. Gulf of Mexico (GOM) is a world-class producer of natural gas from a variety of sources, including primary and secondary microbial methanogenesis and thermogenic sources. The GOM therefore provides an ideal location to test the efficacy of methane clumped isotope geochemistry as a means of deciphering the origins of methane. The GOM is particularly interesting because it has been subjected to extensive salt-diapirism that has allowed for these multiple sources of gas to commingle in certain settings (Beeunas, 2001). This feature makes identifying the origin of the gas more complicated as our current geochemical techniques do not have the fidelity to always deconstruct these mixtures. Here we measure compound-specific carbon and hydrogen isotopes, methane clumped isotope (including $\Delta^{13}CH_3D$ and $\Delta^{12}CH_2D_2$, and their combination of Δ_{18} values) and hydrocarbon and non-hydrocarbon molecular compositions

of natural gases from several petroleum fields in the Gulf of Mexico, in order to characterize the formation mechanism of methane.

2. SAMPLE LOCATION and GEOLOGICAL BACKGROUND

Gas samples were collected from seven different petroleum fields in the Gulf of Mexico: the Galveston 209 field, the Genesis field, the Hoover, Madison, South Diana and Diana fields of the Hoover-Diana mini-basin, the Hadrian North and South Fields and the Julia Field (Figure 1). These fields produce from reservoirs that range in age from Pleistocene through Eocene, and exhibit a range in reservoir temperatures from 42-115^{o}C.

2.1 Galveston Field

The Galveston 209 Field is located 20 miles SE of Galveston, TX in the Galveston protraction area of the Northwestern US Gulf of Mexico in approximately 20 m of water. Hydrocarbons are reservoired in a series of at least 20 Lower to Middle Miocene stacked sands in low-relief structural traps that are sealed by fault-dependent closures juxtaposed against shales. Wells in the field produce dominantly gas, with three key oil-producing reservoir intervals. The reservoirs in the Galveston 209 fluids are thought to be sourced from Eocene aged source rocks that contain dominantly terrestrial organic matter, which generally produces relatively large proportions of gas and lower proportions of oil (Hood, 2002).

2.2 Genesis Field

The Genesis field is located in the Green Canyon blocks of 160, 161 and 205 in the central US Gulf of Mexico in water depths of approximately 700-800m. The field lies on the eastern flank of a salt-cored ridge that defines the western margin of the Popeye-Genesis mini-basin. The Genesis field produces oil with solution gas from stacked Pliocene through Pleistocene deep-water reservoirs (Sweet, 2007; Barry et al., 2018) with perforation depths of 3000-4200m. The range of reservoir temperatures is 63-82^{o}C. The Genesis oils are sourced from the Upper Jurassic interval, most likely the Tithonian marl comprising dominantly marine organic matter (Hood, 2002).The oils are hosted in stratigraphic traps that pinch out against a salt diapir. The reservoirs are thought to be relatively disconnected both laterally and vertically (Sweet, 2007) and consistent with other reservoir connectivity in the greater Green Canyon area (Rowan, 1998). These relationships have been previously described in the larger Green Canyon area (Rowan, 1998).

2.3 Hoover and Diana Fields

The Hoover and Diana fields in the Hoover-Diana mini-basin are located at the intersection of the Alaminos Canyon and East Breaks protraction areas in the western US Gulf of Mexico in water depths of approximately 1400–1500m. Oil and oil-solution gas are hosted in Plio-Pleistocene reservoirs, and are thought to be sourced from a Tertiary marine source interval (Hood, 2002). The fields comprise of dominantly oil in the Hoover fields in the eastern portion of the mini-basin, with dominantly gas in the Diana and South Diana fields in the western portion of the mini-basin. Reservoir temperatures range from approximately 50^{o}C at Diana to approximately 68^{o}C at Hoover.

2.4 Hadrian Fields

The Hadrian North and South fields are located in the Keathley Canyon protraction area of the central US Gulf of Mexico in approximately 2300 m water depth. The fields contain dominantly oil in the south, and dry gas in the north with a small oil rim. Similarily to the Genesis Basin, the fields in the Hadrian fields are also sourced from the Upper Jurassic source interval. The hydrocarbons are produced primarily from Pliocene sands in a fault dependent structural trap that lies beneath a salt canopy.

2.5 Julia Field

The Julia field is located in the Walker Ridge protraction area of the central Gulf of Mexico in water depths of more than 2100 m. The field produces oil and oil-solution gas hosted in roughly 300m of Eocene sands from a structural trap that lies beneath a thick salt canopy. The fluids are thought to be sourced from the Upper Jurassic source rock (Hood, 2002).

3. METHODS

3.1 Methane purification

Methane (CH_4) was purified from mixed gas samples using previously described cryogenic methods (Stolper et al., 2014b). Briefly, approximately 60 μmol of natural gas was sampled. Gas samples were introduced to a vacuum glass line and exposed to liquid nitrogen to trap H_2O, CO_2, and H_2S. The gases in the headspace (including CH_4, O_2, and N_2) were then exposed and transferred to a 20 K cold trap. Residual gases in the headspace (mostly He and H_2) were pumped away. The cold trap was then sealed, heated to 80 K, cooled to 45 K, and opened to vacuum to remove N_2 and O_2. This step was repeated until <2.67 Pa of gas remained in the cold trap at 45 K, corresponding to a purity of CH_4 of 99.8% (Stolper et al., 2014a). The cryostat was then heated to 70 K, and CH_4 was transferred to a Pyrex™ breakseal containing molecular sieve (EM Science; type 5A) immersed in liquid N_2. Samples were heated to 135ºC for 2 hours to fully liberate methane from the molecular sieve prior to introduction into the Thermo Finnegan MAT 253 Ultra. This heating has been shown to not alter the isotopic composition of the gas (Stolper et al., 2014b).

3.2 Methane stable isotope measurements

δD_{VSMOW}, $\delta^{13}C_{VPDB}$, and Δ_{18} of methane were measured using a prototype model of the Thermo Fisher IRMS Ultra, using previously described methods (Stolper et al., 2014a). δD and $\delta^{13}C_{VPDB}$ values are expressed as $\delta D_{VSMOW} = ((R^2H_{sample}/R^2H_{VSMOW})-1)*1000$, and $\delta^{13}C_{VPDB} = ((R^{13}C_{sample}/R^{13}C_{VPDB})-1)*1000$, where $R^2H=[D/H]$, $R^{13}C=[^{13}C/^{12}C]$), VSMOW is Vienna Standard Mean Ocean Water (VSMOW) and VPDB is Vienna Pee Dee Belemnite. Clumped isotope compositions are expressed using Δ_{18} notation, where $\Delta_{18}=((^{18}R/^{18}R^*)-1)*1000$, $^{18}R=[^{13}CH_3D]+[^{12}CH_2D_2]/[^{12}CH_4]$ and $^{18}R^*=(6*[R^2H]^2)+(4*R^2H*R^{13}C)$. $^{18}R^*$ is the ^{18}R value expected for a random internal distribution of isotopologues given the $\delta^{13}C_{VPDB}$ and δD_{VSMOW} value of the sample (Stolper et al., 2014a). The specified isotope ratios are measured from the corresponding ion beam current ratios and standardized by comparison with a standard of known composition. Δ_{18} data are reported as per mil (‰), where 0‰ refers to a random distribution of methane isotopologues, and positive values indicate enrichment in the clumped isotope species relative to the random distribution. We present measurement uncertainties for individual samples as one standard error of the internal measurement variability for a single measurement

(1σ SE). Reported uncertainties for inferred temperatures are propagated from the 1σ errors for Δ_{18} values and are typically ~20°C. Finally Δ_{18} values can be related to an apparent temperature (K) via the equation: $\Delta_{18}=-0.0117*(10^6/T^2)+0.708*(10^6/T^2)-0.337$. We refer to such calculated temperatures as 'apparent temperatures' to indicate that they may indicate geophysical temperatures of methane formation (as appears generally to be true for natural gas reservoirs; (Douglas et al., 2017)), or might instead reflect a kinetic isotope effect associated with some non-equilibrium chemical process. Most of the samples reported in this paper report clumped isotope compositions of methane using the Δ_{18} index that combines contributions from $^{13}CH_3D$ and $^{12}CH_2D_2$; approximately 98% of the mass 18 signal comes from $^{13}CH_3D$, which dominates variations in Δ_{18} value for methane sources of interest to this study.

3.2.1 Methane clumped isotope analysis on the production-type Ultra

We measured $\Delta^{12}CH_2D_2$ and $\Delta^{13}CH_3D$ (i.e., as separate variables, rather than combined as a Δ_{18} value) for 4 of the samples using a 2-day method. We have since developed a 1-day method that will be presented in a future publication. These measurements were made on a separate aliquot of methane (i.e., different from the aliquot measured for Δ_{18}) purified from natural gas mixtures using the production model of the Thermo Scientific 253 Ultra, a high-resolution gas source mass spectrometer housed at Caltech. The production model 253 Ultra (hereafter 'Ultra') routinely delivers mass resolving power (5%/95% definition) between 45,000 and 50,000 at the highest resolution setting (high resolution slit with HR+ aperture setting). The Ultra also features a 9-collector array, 4 of which are equipped with either compact discrete dynode (CDD) or secondary electron multiplier (SEM) as ion counters.
Each analysis of methane involves determination of 4 isotopologue ratios: $^{12}CH_2D_2/^{12}CH_4$, $^{13}CH_3D/^{12}CH_4$, $^{12}CH_3D/^{12}CH_4$ and $^{13}CH_4/^{12}CH_4$, in which $^{13}CH_3D/^{12}CH_4$ and $^{13}CH_4/^{12}CH_4$ are measured simultaneously. Samples are analyzed in a dual-inlet system versus an intra-laboratory standard, CIT-1. (D. A. Stolper et al., 2014) This standard has $\delta^{13}C=-42.88‰$, $\delta D=-175.5‰$, $\Delta^{12}CH_2D_2=7.6‰$ and $\Delta^{13}CH_3D=2.90‰$ (based on comparison with external reference gases and methanes equilibrated at known temperature in our laboratory; see Stolper et al., 2014).

3.2.2 $^{12}CH_2D_2/^{12}CH_4$ measurement

In this analysis, $^{12}CH_2D_2$ is registered on the H4 CDD collector of the Ultra. We use the HR entrance slit (5 μm) with standard intermediate aperture for this measurement. Mass resolving power at this configuration is tuned to be 31,000-36,000 (5%-95%). The H4 CDD collector is equipped with a narrow exit slit (40μm) that permits full resolution of the non-methane peaks at mass 18, including $H_2{}^{16}O$, $D^{17}O$, ^{18}O, $^{14}NH_4$ and $^{15}NH_3$. We also achieve separation of the 4 species of methane and adducted methane: $^{13}CH_3D$, $^{13}CH_5$, $^{13}CH_2D_2$ and $^{13}CH_4D$ (Figure 2). The L4 faraday collector is placed in the middle of the high-mass shoulder of the mass-16 peak cluster, such that it is simultaneously counting $^{12}CH_4$. The L4 faraday collector is registered through a $10^{10}\,\Omega$ amplifier.

Each measurement consists of 240 reference-sample acquisition cycles (480 acquisitions total). We execute a peak-center on the $^{13}CH_3D$ peak before each acquisition, and then jump 0.00292 Da to the higher mass to park on the $^{12}CH_2D_2$ peak for integration. Each acquisition integrates the $^{12}CH_2D_2$ intensity over 60s. Pressure re-adjustment is performed every 6 cycles. Normally we perform this analysis with an ion source pressure of 1.8×10^{-7} -2.2×10^{-7} mbar, which yields around 100-120 counts per second on $^{12}CH_2D_2$. We achieve a shot-noise limited external error of 1.0‰ over the entire measurement.

Although the methane isotopologues are visibly resolved from each other in the mass spectrum under the conditions described above, we examined the contribution to the $^{12}CH_2D_2$ signal from the higher-mass tails of $^{13}CH_3D$, $^{13}CH_5$. We mapped the detailed peak shape function on the water peak that has no adjacent interferences and found that the extended tail in the outer mass range disobeys ideal error-function peak shape (showing a 'kink' in a plot of the logarithm of ion intensity vs. mass position). Since peak shape functions are invariant across ion species (observed from direct comparison), we can apply the peak shape function of water to constrain the tailing of $^{13}CH_3D$ and $^{13}CH_5$. We estimate that the tail of $^{13}CH_3D$ contributes 0.5-1counts per second and the tail of $^{13}CH_5$ contributes 1.5-2.5 counts per second to the center mass of $^{12}CH_2D_2$ under the typical conditions (pressure, tuning) of our measurement. These contributions are significant, so we implement a quantitative correction scheme to revise the raw $^{12}CH_2D_2/^{12}CH_4$ ratio based on contributions from the low-intensity tails of these nearby peaks. Specifically, we measure the adduct line ($^{13}CH_5/^{12}CH_4$ vs. $^{12}CH_4$ to obtain the intensity of the $^{13}CH_5$ and apply the peak shape function based on measurements of the water peak to obtain the intensity of the $^{13}CH_5$ tail at the position of the $^{12}CH_2D_2$ peak. Then we calculate the intensity of $^{13}CH_3D$ by multiplying an isotopologue abundance ratio and applying the peak shape function to obtain the intensity of the its tail at the position of the $^{12}CH_2D_2$ peak. We apply this correction to every acquisitions in the measurement.

3.2.3 $^{12}CH_3D/^{12}CH_4$ measurement

In this analysis, $^{12}CH_3D$ is registered on the H4 CDD collector of the Ultra. We use the HR entrance slit (5 μm) with HR+ intermediate aperture in for this measurement. Mass resolving power at this configuration is tuned to be 45,000-50,000 (5%-95%). At this mass resolution, every isobar at mass 17 is fully resolved from each other. The L4 collector (registered with a 10^{11} Ω amplifier) is simultaneously used to count $^{12}CH_4$ in the middle of the high-mass shoulder of the mass-16 peak cluster.

Each measurement consists of 200 reference-sample acquisition cycles (400 acquisitions total). We execute a peak-center on the $^{12}CH_3D$ peak before each acquisition. Each acquisition integrates the $^{12}CH_2D_2$ intensity over 20s. Pressure re-adjustment is performed every 5 cycles. Normally we perform this measurement at an ion source pressure of 5×10^{-8} -8×10^{-8} mbar, which yields around 30,000-50,000 counts per second on $^{12}CH_3D$. We achieve an external error (based on the standard error of all cycles) of 0.15‰.

3.2.4 $^{13}CH_3D/^{12}CH_4$ and $^{13}CH_4/^{12}CH_4$ measurement

In this analysis, $^{13}CH_3D$ is registered on the H3 CDD collector of the Ultra. We use the HR entrance slit (5 μm) with standard intermediate aperture for this measurement. Mass resolving power at this configuration is tuned to be 28,000-31,000 (5%-95%). The H3 collector has a wider exit slit (800μm) so we integrate $^{13}CH_3D$ in the middle of the low-mass shoulder of the mass 18 peak top. The L4 collector is simultaneously counting $^{12}CH_4$ in the middle of the high-mass shoulder at mass 16 and the center collector is simultaneously counting $^{13}CH_4$ in the middle of the low-mass shoulder at mass 17.

Each measurement consists of 120 reference-sample acquisition cycles (240 acquisitions total). We execute a peak-center on the water peak every 4 acquisitions. Each acquisition integrates the $^{13}CH_3D$ intensity over 30s. Pressure re-adjustment is performed every 6 cycles. Normally we perform this measurement with an ion source pressure of 9×10^{-8} -1.5×10^{-7} mbar, which yields around 3000-6000 counts per second on $^{13}CH_3D$. We achieve a shot-noise limited

external error of 0.25‰ on $^{13}CH_3D/^{12}CH_4$ and 0.01‰ on $^{13}CH_4/^{12}CH_4$ over course of the entire measurement.

Contaminants of $H_2{}^{16}O$, NH_4 and $^{13}NH_3$ contribute to the background where we integrate $^{13}CH_3D$. We measure the intensity of such contaminant background by jumping the magnet by 0.004Da to the lower mass side from measurement mass before and after the whole measurement. This background is scaled by an independently determined background shape to derive true background under measurement mass. Then we subtract it from raw $^{13}CH_3D$ counts, which is usually around 30-50 counts per second.

3.2.5 Calibrations curves used for $\Delta^{12}CH_2D_2$ and $\Delta^{13}CH_3D$

Four samples were selected for additional analysis on the production model of the Thermo Fisher IRMS Ultra. δD_{VSMOW} and $\delta^{13}C_{VPDB}$ values are expressed similarly to the data from the prototype Ultra. $\Delta^{13}CH_3D$ and $\Delta^{12}CH_2D_2$ are reported as $\Delta^{13}CH_3D = (((^{13}CH_3D/^{12}CH_4)_{sample}/(^{13}CH_3D/^{12}CH_4)_{standard} - 1)*1000$, and $\Delta^{12}CH_2D_2 = (((^{13}CH_2D_2/^{12}CH_4)_{sample}/(^{12}CH_2D_2/^{12}CH_4)_{standard} - 1)*1000$. $\Delta^{13}CH_3D$ can be correlated to temperature using the equation: $\Delta^{13}CH_3D\ (T) \approx 1000 \ln (1 + 0.0355502/T - 433.038/T^2 + 1270210.0/T^3 - 5.94804x10^8/T^4 + 1.196630x10^{11}/T^5 - 9.07230x10^{12}/T^6)$ while $\Delta^{12}CH_2D_2$ can be correlated to temperature using the equation: $\Delta^{12}CH_2D_2\ (T) \approx 1000 \ln (1 + 0.183798/T - 785.483/T_2 + 1056280.0/T^3 + 9.37307x10^7/T^4 - 8.919480x10^{10}/T^5 + 9.901730x10^{12}/T^6)$ (Young et al., 2017). When methane is formed at thermodynamic equilibrium, $\Delta^{13}CH_3D$ and $\Delta^{12}CH_2D_2$ exhibit positive values that approach 0‰ at high temperatures.

3.3 C_2-C_5 hydrocarbon gas component stable isotope measurements

Molecular compositions of gas samples were measured using gas chromatography (GC) in Isotech Laboratories in Champaign, Illinois. The gas samples are first prepared for analysis by injecting an aliquot of gas into an offline prep system, which consists of a GC system equipped with both thermal conductivity and flame ionization detectors. The GC system separates the individual hydrocarbons and a cupric oxide furnace then combusts each component into CO_2 and H_2O. The gases are then further purified and sealed into pyrex tubing using a vacuum collection manifold. The H_2O is then reacted with zinc turnings to generate H_2 gas. The CO_2 and H_2 are separately introduced into a dual inlet IRMS system, where the isotope ratios are accurately measured.

3.4 Bulk Oil stable isotope measurements

Approximately 0.2mg of oil is weighed into a tin capsule for carbon isotope analysis, and approximately 0.5mg weighed into a silver capsule for hydrogen isotopic analysis. The carbon isotope sample is then loaded into an Elemental Analyzer (EA) while the hydrogen sample is loaded into a Thermo-Chemical Elemental Analyzer (TCEA). The samples are combusted and purified within the EA of TCEA system itself. The outlets of the EA and TCEA are connected to a Thermo Delta V Plus IRMS which measures the isotopic ratios.

4. RESULTS

$\delta^{13}C$ and δD_{VSMOW} of C_2-C_5 hydrocarbon gases (Figure 3), as well as methane δD, $\delta^{13}C$, Δ_{18}, $\Delta^{13}CH_3D$ and $\Delta^{12}CH_2D_2$ (Figure 4-7 and Table 1 and 2), $\delta^{13}C$ of CO_2 (Table 2) and bulk oil

C and H isotope analyses (Table 3) from the Gulf of Mexico samples are reported here. The $\delta^{13}C_{VPDB}$ of CH_4 ranged from -40 to -64‰. Typically $\delta^{13}C$ values <-60‰ are considered to be indicative of a microbial origin while values >-50‰ are considered indicative of a thermogenic origin (Whiticar, 1999). The gases from the Gulf of Mexico fall near the boundary between those ranges and do not provide unequivocal evidence for the origin of the methane. The δD_{VSMOW} of CH_4 ranged from -147 to -300‰, which along with the $\delta^{13}C$ values falls in the transition zone of thermogenic and microbial gas in the Whiticar plot (Whiticar, 1999). The Δ_{18}-based apparent temperatures of the suite of gases range from 34-200ºC. Values of $\Delta^{13}CH_3D$ for the four samples measured on the production Ultra range from 2.5-5.4‰, consistent with a range in apparent temperature (45-206˚C) similar to that implied by measurements of Δ_{18} on the prototype Ultra. These apparent temperature ranges are consistent with the range of geophysical temperatures experienced by these gases, from maximum source rock temperatures in the 'gas window' (ca. 150-200 ˚C) down to measured reservoir temperatures (42-115 ˚C).

Values of $\Delta^{12}CH_2D_2$ range from -0.1 to 11.4‰. The sample from Galveston that appears based on context and other geochemical properties to be primarily thermogenic in origin (sample Galveston B7D) has a $\Delta^{12}CH_2D_2$ value of 2.5‰, consistent with thermodynamic equilibrium at temperatures consistent with thermogenic gas production. Thus, it meets the criteria of an equilibrated thermogenic gas whose clumped isotope apparent temperature reflects the geophysical temperature of gas generation (a common finding for analyses of $\Delta^{12}CH_2D_2$ and $\Delta^{13}CH_3D$ from conventional thermogenic gases; (Young et al., 2017; Giunta et al., 2019)). The other three samples selected for $\Delta^{12}CH_2D_2$ measurement were chosen from suites of gases having geochemical properties suggesting the presence of a component of microbial gas, including relatively low $\delta^{13}C$ and/or δD and elevated gas dryness, and Δ_{18} values suggesting apparent temperatures of less than 100 ˚C. All three of these samples exhibit $\Delta^{12}CH_2D_2$ values lower than anticipated for thermodynamic equilibrium at any plausible gas generation or storage temperature, and clearly falling off the correlation of $\Delta^{12}CH_2D_2$ vs. $\Delta^{13}CH_3D$ defined for thermodynamic equilibrium (we discuss in the following section whether one or both of these two properties are likely controlled by the possible non-equilibrium processes). The additional constraints offered by $\Delta^{12}CH_2D_2$ help confirm a significant contribution of microbial methane which would not have been more difficult with Δ_{18} or $\Delta^{13}CH_3D$ measurements alone.

The $\delta^{13}C_{VPDB}$ and δD_{VSMOW} values of C_2-C_5 hydrocarbon gases range from -25 to -45‰ for $\delta^{13}C$ and -90 to -220‰ for δD_{VSMOW} (Table 2 and Figure 5). The $\delta^{13}C_{VPDB}$ and δD_{VSMOW} for C_2-C_5 gases in Galveston, Genesis and Diana Hoover are similar to typical thermogenic oil-associated gases (Whiticar, 1994) while associated and solution gases from the Hadrian fields and the Julia field are more consistent with a mixture of secondary microbial gas and oil-solution gas (Milkov and Dzou, 2007). The thermal maturity of these gases is estimated at 0.2 – 1.8% vitrinite reflectance equivalent (Ro_{eq}) based on the $\delta^{13}C_{VPDB}$ of C_2 and C_3 using the equations of (Whiticar, 1994). These estimates would suggest a range in the maturity of the source interval for these gases from immature to upper gas-window maturity for Type 2 organic matter (Tissot, 1984). Significant hydrocarbons are not formed from an immature source (0.2% Ro_{eq}). However, from a bulk C isotope perspective, we consider it possible that elevated maturity gases (e.g. > ~1.5% Ro_{eq}) could be present within our sample suite. $\delta^{13}C$ and δD of crude oil in Genesis was also measured and $\delta^{13}C$ values fell in a narrow range of -27 to -27.2‰, while δD values fell in a narrow range of -100 to -103‰.

5. DISCUSSION

The findings presented in Section 4 indicate that there is significant variability in isotopic properties of natural gases from the GOM, and that those variations are generally well correlated for individual suites of geographically related samples but not for the entire sample suite as a whole. This suggests that there are three or more end member compositions to the GOM gases as a whole, but that individual suites can be described using just two such end members — i.e., individual reservoirs exhibit relatively simple isotopic systematics, but those systematic trends reflect local components or processes rather than GOM-wide uniform components or processes. Thus, any interpretation of the stable isotope data for GOM natural gases should focus on understanding local, closely related suites, and a broader understanding of the basin as a whole will emerge only by recognizing how properties and processes that control isotopic compositions vary with geology, stratigraphy, hydrocarbon generation and burial history. The following discussion first considers guidelines we will use to interpret the properties and origins of the end members of trends in isotopic properties for suites of related gases (Section 5.1), and then applies those principles to interpret the origins of gases from the suites examined in this study (sections 5.2-5.5).

5.1 Properties and origins of end-members of GOM gas isotopic trends

5.1.1 *Recognition of end members*

Natural gases associated with Gulf of Mexico petroleum reserves are often suspected of being mixtures of thermogenic C_1-C_5 gases and microbially produced methane. In each basin, we selected thermogenic end-member temperatures by examining the maturity of accompanying oil samples, $\%Ro_{eq}$, and thermal history models for both the reservoir and source rock intervals. We selected microbial end-members by examining thermal models to consider reasonable paleo-burial temperatures that would support microbial gas generation and compared those to current reservoir temperatures. We also characterized these end-member gases using the framework from for conventional systems (Bernard et al., 1978; Whiticar, 1999).

5.1.2 *Equilibrium vs. non-equilibrium controls of clumped isotope apparent temperatures*

1) If the combined $\Delta^{13}CH_3D$ and $\Delta^{12}CH_2D_2$ values are consistent with the correlation between these properties predicted for thermodynamic equilibrium, this supports the interpretation that this methane is in internal isotopic equilibrium and that the apparent temperature reflects a geological temperature of formation or re-equilibration. This is true of the one clearly thermogenic gas analyzed for both of these clumped isotope indices. If instead the combined $\Delta^{13}CH_3D$ and $\Delta^{12}CH_2D_2$ values are inconsistent with equilibrium we take it as evidence that this methane is not in internal isotopic equilibrium and that one or both of its apparent temperatures (i.e., based on $\Delta^{13}CH_3D$ and $\Delta^{12}CH_2D_2$ values) could differ from the geological temperature of formation or re-equilibration. As discussed in Section 1, some recognized non-equilibrium synthesis processes produce large departures from equilibrium for both of these indices (Young et al., 2017), whereas other non-equilibirum synthesis processes produce large departures from equilibrium only for $\Delta^{12}CH_2D_2$, leaving $\Delta^{13}CH_3D$ relatively unaffected (Dong et al., 2019). Thus, it is possible for such gases the apparent temperature based on the $\Delta^{13}CH_3D$ value is equivalent to, or closely approaches, a geological formation temperature.
2) We compared the clumped isotope apparent temperatures of putative thermogenic end-members for each family of gases to independent constraints on source rock catagenetic temperatures, including the maturity of the accompanying oils and thermal histories reconstructed by basin

models. If the samples yield clumped isotope apparent temperatures that are reproducible and consistent with independent geological constraints, we take this as evidence that they equal or closely approach geological formation temperatures. Note that all recognized mechanisms for producing significant non-equilibrium clumped isotope anomalies (microbial or thermogenic) lead to dramatically too-high apparent temperatures, and are generally associated with large variability in apparent temperature.

3) We compare the clumped isotope apparent temperatures of putative microbial end-members, and pure microbial gases, to independent constraints based on direct observation of well and fluid temperatures and basin thermal models. The ranges of plausible temperatures are generally low and narrow (within tens of degrees of ~50 ˚C), making it improbable that recognized mechanisms for making non-equilibrium biological methanogenic clumped isotope signatures could fortuitously mimic these apparent temperatures.
4) All of the studied gases come from marine (type II kerogen) or mixed marine-terrigenous (type II-III kerogen) source rocks and were hosted in clastic reservoirs in a marine environment. This leads to the expectation of a narrow range in D/H ratios for product methane (Whiticar, 1999). And, recognized processes that create non-equilibrium clumped isotope signatures are typically associated with strong D/H depletions relative to co-existing waters or organic substrates (for methanogenic processes) or enrichments relative to starting methane (for residues of methanotrophy). Thus, δD values for methane that are within the range of typical marine gases and closely similar to other, related gases generally supports the interpretation of clumped isotope compositions equal to or closely approaching those for geological equilibrium, whereas anomalously low δD values support the interpretation that clumped isotope indices may be disturbed by non-equilibrium processes.

5.2 Galveston Basin

The methane extracted from samples from the Galveston 209 field have the highest $\delta^{13}C_{VPDB}$ values of gases examined in this study, ranging from -39 to -42‰ (Figure 3). The Galveston 209 field also has the highest $\delta^{13}C_{VPDB}$ values of the C_2-C_5 gas components in our study area (Figure 3a). The $\delta^{13}C$ of ethane from these reservoirs would predict a source maturity of 1.7 – 1.8% R_o based on the equations of Whiticar (1994). These R_o values suggest contributions of a higher maturity fluid to the reservoir, though we note here these equations are typically only associated with type II kerogen and may therefore not be as accurate for the dominantly terrigenous organic matter that generated these fluids. The δD_{VSMOW} values of the methane in these samples are relatively constant at -150‰, and the apparent temperatures derived from methane Δ_{18} values range from 130-200ºC (Figure 5c). We have analyzed one gas sample for $\Delta^{13}CH_3D$ and $\Delta^{12}CH_2D_2$ and find that the sample is in equilibrium at ~200°C (Figure 6). The gas wetness ($C_1/(C_2+C_3)$) of these samples ranges from 23-30 (Figure 5b), consistent with a dominantly thermogenic origin for these species (Whiticar, 1994).

The $\delta^{13}C_{VPDB}$ and δD_{VSMOW} of the higher n-alkanes (C_2-C_5) decrease approximately linearly with increasing 1/n, where n is the number of carbon atoms per molecule (Figure 3). Such trends are characteristic of gases from thermogenic sources with a similar source maturity (Chung et al., 1988). Decreases in $\delta^{13}C_{VPDB}$ and δD_{VSMOW} of related C_1-C_5 hydrocarbons with increasing 1/n is generally ascribed to a kinetic isotope effect during catagenesis. Cleavage of bonds involving moieties containing only low mass isotopes is generally faster than those in moieties containing high mass isotopes; therefore thermal 'cracking' of larger organic molecules should generally result in ^{13}C and D depletions of the resulting gas products relative to their source compounds. If each gas product is generated by cleavage of a single bond (as a

simplifying assumption), then small product molecules will express more of the associated kinetic isotope effect while larger product molecules will have this effect diluted by the larger number of unfractionated sites. Such trends are characteristic of genetically associated gases generated from the same source rock (Chung et al., 1988; Tang et al., 2000; Ni et al., 2011).

In the suite of Galveston 209 samples we have studied, the expected thermogenic endmember has a $\delta^{13}C_{VPDB}$ of -29.8‰ (based on extrapolating $\delta^{13}C$ values of the C_2-C_4 trend) while the measured $\delta^{13}C_{VPDB}$ values are -41‰. Thus, this line of reasoning would lead us to conclude that the Galveston samples contain abundant microbial methane. For example, if pure microbial gas has a $\delta^{13}C_{VPDB}$ value ranging from -70 to -120‰ (Whiticar et al., 1986) (Figure 4), then we might conclude that the methane in Galveston 209 fluids ($\delta^{13}C_{CH4}$=~-41‰) is 13-29% microbial and 87-71 % thermogenic based on a linear mixing of the concentrations of ^{12}C and ^{13}C of the endmembers ($\delta^{13}C_{microbial}$=-70 to -120‰, $\delta^{13}C_{thermogenic}$=-29.8‰). Additionally, Galveston 209 gases also have a relatively simple monotonic trend of compositions in Figures 5a and 5b, which support a simple two component mixing.

In the absence of any other constraints, the argument laid out above could be seen as reasonable, or at least self-consistent. However, we consider two independent constraints to conclude that the Galveston gases cannot be reasonably interpreted as two-component mixtures of thermogenic and microbial gas. Firstly, if we extrapolate the observed correlation between $\delta^{13}C_{VPDB}$ and δD_{VSMOW} for the measured Galveston 209 methane samples to the model predicted $\delta^{13}C_{VPDB}$ of -29.8‰, it would imply that the δD_{VSMOW} of the thermogenic end member is -118‰. This extraordinarily high value is outside the range of published δD_{VSMOW} for methane from other Gulf of Mexico locations (Sassen et al., 1999; Douglas et al., 2017). Further, the putative thermogenic endmember would be higher in value than high maturity (> 2.0% $R_{o,}$eq) thermogenic methane from the Upper Jurassic Haynesville formation studied previoulsy (Stolper et al., 2014), which is the on-shore equivalent of the proposed source for the nearby Genesis hydrocarbons. Similarly, although the trend of apparent temperature vs. $\delta^{13}C$ is not well defined for this suite, an apparent Δ_{18} temperature in excess of 300 ˚C (calculated by extrapolating $\delta^{13}C_{VPDB}$ to -29.8‰ in a plot of Δ_{18}-temperature vs $\delta^{13}C_{VPDB}$ and calculating corresponding temperature) would likely be required for the thermogenic end member. This high temperature is not a physically plausible temperature of thermogenic methane formation in any system associated with oil, and is well outside the range of predicted source rock temperatures in this region of the GOM (Nunn, 1986). We conclude that the premise of the argument is flawed; that is, while broadly negative slopes in plots of $\delta^{13}C_{VPDB}$ vs. 1/n are generally typical of thermogenic gases, such trends are not sufficiently coherent and predictive to serve as quantitative measures of microbial methane abundance relative to thermogenic inputs. This finding is consistent with results from a recent Monte Carlo modeling study of alkane cracking that demonstrated that deviations from a straight line in the natural gas, or Chung, plot can arise both in early and late stages of hydrocarbon generation as a result of modifications to the site specific isotopic signature of the terminal position of large molecules during thermal breakdown to smaller alkanes (Peterson et al., 2018).The methane clumped methane measurements indicate that methane sampled from Galveston 209 display an apparent equilibrium temperature of 130-200ºC (Figure 5c-d). As microbial methane cannot form at these elevated temperatures (Connan, 1984) and the inferred temperatures are within the range at which thermogenic methane typically forms (~60 to~250 ºC), we believe that the Galveston 209 fluids are predominantly thermogenic in origin and formed during initial catagenic breakdown of organic macromolecules to oil and gas (Figure 8). The 130-200ºC range of apparent methane formation temperatures is higher than the

reservoir temperature of 90-105°C (Figure 5e). This difference is consistent with the gases being generated in a source rock that was ~1-4 km deeper than the current reservoir based on an average Northern Gulf of Mexico geothermal gradient of ~25°C/km (Forrest, 2005) and then having migrated to their current location. This range of temperatures are indeed consistent with source rock maturities that range from the oil window (80 - 160°C) in to the gas window (> 160°C).

5.3 Genesis Field

The solution gases we studied from the Genesis field have methane $\delta^{13}C_{VPDB}$ values ranging from -55 to -65‰— a range that includes values commonly associated with microbial gas, but is also consistent with a thermogenic origin (Figure 4). The $\delta^{13}C_{VPDB}$ and δD_{VSMOW} of C_2-C_5 gases are consistent with oil-associated thermogenic gases (Figure 3) and the Δ_{18} values of the studied samples varied widely from 3.9-6‰, corresponding to apparent temperatures ranging from 27 to 112°C (Figure 5c). The gas wetness ($C_1/(C_2+C_3)$ of these gases ranges from 7-12 (Figure 5b) and are also consistent with a thermogenic origin.

The gases in the Genesis field are from two unconnected producing intervals - the upper Pliocene and Pleistocene reservoirs respectively. The gases from the Pliocene reservoirs have Δ_{18} apparent temperatures (27 to 41°C) that are lower than the current reservoir temperatures (~ 81°C), and are relatively low in $\delta^{13}C$, averaging near -63‰. These observations of the Pliocene reservoir are best explained by microbial methane generation at depths shallower than the current reservoir depth in the geologic past, followed by burial transporting the methane and any associated fluids to its present depth. Genesis oils additionally exhibit evidence for biodegradation (Sassen et al., 2003), suggesting that the microbial methane is a mixture of primary and secondary generation associated with the biodegradation of oil. The narrow range in apparent temperatures for gases from different Pliocene reservoir intervals strongly suggests that the methane in these fluids is dominated by microbial methane, with little or no thermogenic additions. If oils with associated dissolved thermogenic methane migrated in to the reservoir after this initial generation of microbial methane at temperatures of 25 - 35°C, one would expect to see higher apparent temperatures as a result of the mixing of early microbial methane with later thermogenic methane. However since there is a small range in methane apparent temperature, we believe the methane in these fluids must be mostly microbial (Figure 8). Invoking a microbial addition to the Pliocene reservoir might seem contradictory as the Pliocene gases have $C_1/(C_2+C_3)$ values of ~11, and environments affected by microbial methanogeneseis are generally expected to have high $C_1/(C_2+C_3)$ values. However, mixing relationships between two sources of different $C_1/(C_2+C_3)$ values indicates that the resultant mixture is relatively insensitive to the high $C_1/(C_2+C_3)$ source. For example, a 10-50% addition of microbial gas $C_1/(C_2+C_3)$=10,000) to a thermogenic gas $C_1/(C_2+C_3)$==10) will only change the resultant gas' $C_1/(C_2+C_3)$=values by 1-12 (Etiope and Sherwood Lollar, 2013). This reservoir is an instance where by interpreting the temperature range in the context of a thermal history for a reservoir, one is able to place relative time constraints of oil migration into the Pliocene reservoirs given the requirement from methane clumped isotopes for an oil charge at temperatures below 35°C.

In contrast, the gases contained in Pleistocene age sediments have Δ_{18} apparent temperatures (57-112 °C) that range from equal to the reservoir temperature to 10's of degrees hotter than the reservoir temperature. These Δ_{18}-temperatures along with $\delta^{13}C_{VPDB}$ values of -55 to -60‰ are consistent with the reservoir containing a mixture of thermogenic gas produced in the Eocene source rock at depths greater than the reservoir interval and microbial gas produced

either in the reservoir or, potentially, at slightly shallower depths than the current reservoir depth during burial (Figure 8). The upper temperature constraint for the thermogenic end-member of ~120°C in this mixture suggests lower to main stage oil window maturity (Sweeney, 1990, p.1), consistent with observations from molecular geochemistry of representative Genesis oils providing independent constraints on thermal maturity (see supplementary information). However in the absence of $\Delta^{12}CH_2D_2$ measurements we cannot rule out a contribution of microbial gas to this measurement and a fortuitous thermogenic end member temperature that would be consistent (though a little low) with methane generation temperatures predicted by the basin model.

One unusual feature of the Genesis gases is that the δD_{VSMOW} measurements of methane are nearly constant at δD_{VSMOW}=-193.4±2.5‰ (1σ standard deviation). It is difficult to understand how such constant δD_{VSMOW} values could result from mixing between thermogenic and microbial methane that vary widely in $\delta^{13}C_{VPDB}$ and generation temperature because such ranges in $\delta^{13}C_{VPDB}$ and temperature are usually associated with large ranges in δD (Figure 3) (Douglas et al., 2017). One way that the constancy of δD_{VSMOW} values across both the Pliocene and Pleistocene gases could be resolved is if the deuterium content in the methane is buffered by an abundant hydrogen containing component in the natural gas system. We tested the plausibility of various hydrogen containing compounds (water, clay, oil and other hydrocarbons) to buffer the methane δD_{VSMOW} values by exploring the range of methane δDs that are predicted for methane equilibration with each of these compounds given the methane temperatures. There have been no δD_{VSMOW} measurements of water in the Genesis field, however in the nearby Mississippi Canyon protraction, the δD_{VSMOW} of formation waters have been measured in the Miocene sands of the Tubular Bells and found to be -16 to -19‰ (VSMOW) (Franks and Uchytil, 2016). If the waters in the Genesis Basin are similar to the waters measured in the Tubular Bells, methane equilibration with water at the measured methane temperatures of 27-112°C would result in methane δD_{VSMOW} ranging from -237 to -178‰ VSMOW. This predicted range is much larger than our measured range and argues against water being the dominant buffering component. Similarly, methane equilibration with kaolinite and H_2 is highly temperature dependent. Methane buffered by kaolinite would result in a 65‰ range in methane δD (Gilg and Sheppard, 1996) while methane buffered by H_2 (Horibe and Craig, 1995) would produce a 127‰ range in methane δD given the range in observed methane temperatures. The narrow range of measured methane δD argues against H_2 or clay buffering methane.

We can also calculate the equilibrium fractionation between δD_{VSMOW} of methane and a longer-chain *n*-alkane that can be taken as representative of oil which is $C_{11}H_{24}$ for this exercise. We choose undecane as it is the longest n-alkane we are aware of with calculated isotopic partition function ratios (Wang et al., 2009a). The equilibrium hydrogen isotope fractionation between methane and $C_{11}H_{24}$ at corresponding methane temperatures ranges between 55 to 88‰. We have measured the dD of the bulk oil fraction at Genesis and find that the δD_{VSMOW} of bulk oil is between -100 to -103‰ (Table 3). If we assume that $C_{11}H_{24}$ will have a similar dD as the bulk oil fraction, we calculate the methane equilibrated with $C_{11}H_{24}$ at Genesis should have a range in dD values of -149 to -179‰ (VSMOW). This range again is much larger than our measured range of δD_{VSMOW} of methane and argues against oil buffering the methane.

The absolute value of the slope of measured methane δD versus methane temperature 0.074±0.02) is much smaller than the absolute value of the slopes predicted for methane after equilibration with water (0.69±0.03), H_2 (2.79±0.09), kaolinite (0.57±0.03) and oil (0.47±0.01).

We investigate the temperature dependence of the equilibration of δD of CH_4 with various organic moieties in alkanes, alkenes, ketones, carboxylic acid, alcohols and ethers (Wang et al., 2009b). We find a large range in slopes (change in δD versus change in temperature) for methane equilibration with the various moieties, ranging from 1.6 to 0.22. However, none of the moieties we investigated had a slope consistent with our observations. We conclude that our data must be explained by fortuitous mixing between endmembers that are almost identical in δD: a thermogenic endmember with a δD of -200‰ and a microbial endmember with a δD of -190‰.

5.4 Hoover-Diana fields

The conventional oil-associated and solution gases from the Hoover, Madison, Diana and South Diana fields in the Hoover-Diana mini-basin vary in $\delta^{13}C_{VPDB}$ of methane from -56 to -60‰ — spanning an ambiguous range at the border of microbial and thermogenic gases (i.e., Whiticar, 1994), and vary in δD_{VSMOW} of methane from -192 to -202‰ — a modest range similar to that seen in the Genesis field (Figure 3). Also similarly to the Genesis field, the Δ_{18} values of the studied samples vary widely from 3.8-5.3‰ with the methane derived temperatures varying from 52 to 118ºC (Figure 5c and 7). Two samples from this suite were analyzed for $\Delta^{13}CH_3D$ and $\Delta^{12}CH_2D_2$. The gases have $\Delta^{13}CH_3D$-temperatures of 83°C and 116°C and one negative $\Delta^{12}CH_2D_2$ value which does not correspond to a temperature and another with a $\Delta^{12}CH_2D_2$-temperature of 346°C. The gas wetness ($C_1/(C_2+C_3)$) ranges from 10-17 (Figure 5b), consistent with a thermogenic origin.

The Δ_{18}-based apparent temperatures in Hoover-Diana are significantly correlated with $\delta^{13}C_{VPDB}$ (as for the Genesis suite), but in this case increase with decreasing $\delta^{13}C_{VPDB}$. This finding is counter intuitive because thermogenic gases tend to rise in $\delta^{13}C$ with increasing maturity (and therefore, typically with rising temperature), and microbial gases tend to be lower in $\delta^{13}C$ and formation temperature than thermogenic gases. The rising $\delta^{13}C_{VPDB}$ with rising maturity can reflect a trend in reaction progress rather than reaction temperature (Rooney et al., 1995) or may reflect a secondary microbial process (Milkov and Dzou, 2007).

It is known that some microbial gases are higher in $\delta^{13}C_{VPDB}$ than the lowest $\delta^{13}C_{VPDB}$ seen for thermogenic gases (Milkov, 2011; Milkov and Dzou, 2007). Previous research has shown that thermophilic methanogens (environments between 50-75 °C) produce methane with relatively high $\delta^{13}C_{VPDB}$ values ($\delta^{13}C_{VPDB}$~-30‰) compared to mesophilic organisms (environments < 50 °C), which is consistent with our observations (Valentine et al., 2004) although it is not clear how abundant thermophillic methanogens are in this setting. Microbial methane enriched in ^{13}C compared to the expected thermogenic methane (as determined from a Chung plot) has also previously been seen (Milkov and Dzou, 2007) near the Walker Ridge in the Gulf of Mexico and is thought to be due to the addition of secondary microbial methane enriched in ^{13}C. Secondary microbial methane generation occurs anaerobically and involves the microbial degradation of hydrocarbons or high molecular weight compounds to CO_2 and the subsequent reduction of the resulting CO_2 to methane. This process results in more heavy-isotope enriched methane than primary microbial methane.

We suggest that the compositional trends seen in Hoover-Diana samples (Figure 5 and 7) could be consistent with either of two scenarios: (1) The gases currently in the reservoir could be mixtures of thermogenic gas generated at greater depths at temperatures of ~120ºC but also relatively early in the oil and gas generation process, and low maturity thermogenic gas that

formed in the reservoir at temperatures likely greater than 50°C by continued cracking after migration to a shallower depth. This hypothesis is permitted because the minimum temperature observed in Hoover-Diana gases is near the lower limit of, but still within, the range of thermogenic methane production. However, we believe this idea is unlikely as generation of hydrocarbons in the Diana Hoover reservoir is unlikely as the reservoir facies is a fine-grained, deep-water, sandstone (Sullivan, 2002; Sullivan and Templet, 2002) which is not conducive to the levels of organic-matter enrichment required to produce hydrocarbons. Unfortunately, no TOC measurements are available from the reservoir in this study. Or (2) the trends in Figure 5 and 7 could reflect mixing between a thermogenic end-member generated in the oil window at 120˚C at depths greater than the current reservoir, with a microbial end member generated by oil biodegradation at the current reservoir temperature and having a $\delta^{13}C_{VPDB}$ of about -56 ‰. The temperature constraint here on the thermogenic end-member of 120˚C is within analytical uncertainty of the present day temperature of the Eocene source rock estimated from a 1-D thermal history of the Mid-Eocene interval derived from a basin model developed in the vicinity of the Hoover-Diana fields (see supplementary information).

The curves plotted in Figures 5 and 7 illustrate these hypotheses using a mixing model where we assume one component is the gas closest to the current reservoir temperature, representing either in situ thermogenic production or more likely in situ microbial production of methane, and the warmest, most depleted in $\delta^{13}C_{VPDB}$ gas to be a deeper sourced thermogenic endmember. We analyzed two samples with the hottest Δ_{18}-temperatures, from our thermogenic endmember, for $\Delta^{13}CH_3D$ and $\Delta^{12}CH_2D_2$. We find that our mixing model and data agree well with each other for $\delta^{13}C_{VPDB}$, δD_{VSMOW}, Δ_{18}, and $\Delta^{13}CH_3D$, indicating that the Hoover-Diana fields can be considered to be a mixture between two endmember gases, one produced in situ at ~50°C and another generated deeper at ~120°C prior to migrating upwards and mixing at the current reservoir conditions (Figure 8). Interestingly, our model does not agree with an equilibrated biogenic $\Delta^{12}CH_2D_2$ endmember but rather indicates the microbial endmember must be unequilibrated at -20‰. A unequilibrated microbial signature is not surprising and has been seen before in natural and laboratory microbial cultures (Young et al., 2017; Giunta et al., 2019). Future work is required to characterize the $\Delta^{12}CH_2D_2$ signature of this disequilibrated microbial $\Delta^{12}CH_2D_2$ endmember.

5.4 Hadrian and Julia fields

The gases from the Julia (Walker Ridge) and Hadrian fields (Keathley Canyon) are both generated from the same source rock as the gases in the Genesis basin (see Hood et al., 2002). However, there are distinct features in both Hadrian and Julia gases that are unique to each field and different from the Genesis field gases.

Hadrian methane has low $\delta^{13}C_{VPDB}$ values of -55 to -60‰ and δD_{VSMOW} values ranging from -173 to a remarkably low value of -237‰ (Figure 4). Two of the samples (associated gases that overlie a biodegraded oil leg) have low Δ_{18} apparent temperatures of 30-50ºC while a third (solution gas in unbiodegraded oil) has a higher apparent temperature of 100ºC (Figure 3). These fluids exhibit a range in gas wetness ($C_1/(C_2+C_3)$) of 3 to 77 (Figure 5b). We analyzed one associated gas for $\Delta^{13}CH_3D$ and $\Delta^{12}CH_2D_2$ and found a $\Delta^{13}CH_3D$-temperature of 46°C and a $\Delta^{12}CH_2D_2$-temperature of 99°C. These fluids exhibit a range in gas wetness $C_1/(C_2+C_3)$ of 3 to 77 (Figure 4b).

Julia methane samples have low $\delta^{13}C_{VPDB}$ values of -57 to -59‰, and also have very low δD_{VSMOW} values ranging from -267 to -300‰ (Figure 4), yet have Δ_{18} apparent temperatures that

are far higher, ranging from 123-180°C (Figure 5). These samples represent the wettest fluids of the suite of gases, with gas wetness ($C_1/(C_2+C_3)$) ranging from 1.0-1.5 (Figure 5b).

Similarly to the Genesis field, the Hadrian gases display a range of Δ_{18}-temperatures relative to the reservoir temperature (Stolper et al., 2014a). One sample is in equilibrium with the reservoir temperature (48°C), suggesting it formed in situ. This sample has a $\Delta^{13}CH_3D$-temperature of 46°C and a $\Delta^{12}CH_2D_2$-temperature of 99°C. This sample also has a $C_1/(C_{2+}C_3)$ ratio of 78, the highest ratio of all the gases in the sample suite, suggesting it has a higher relative proportion of microbial gas compared to other gases in this GOM suite. The different clumped isotope temperatures suggests a slight disequilibrium in this sample. This disequilibrium signature could be associated with a microbial component in the gas which has previously been shown to be associated with depleted $\Delta^{12}CH_2D_2$ values (Young et al., 2017; Giunta et al., 2019). Another sample is slightly cooler (34°C) with a relatively low $\delta^{13}C_{VPDB}$ value (-60‰) and a $C_1/(C_{2+}C_3)$ of 43, also suggesting a significant component of microbial gas is present in the reservoir. Both of these samples were taken from dominantly gas fields, suggesting that microbes have biodegraded an initial oil charge at or near the present day reservoir temperatures, producing secondary microbial methane with these observed Δ_{18} temperatures (Figure 8). The third gas has a depleted δD_{VSMOW} value of -237‰ and a Δ_{18}-temperature of 101°C, much hotter than the reservoir temperature of 60°C. This sample is present as a solution gas in associated oil, and we consider this to reflect a thermogenic end-member among this set of gases (Figure 8). The apparent hot methane generation temperature and depleted in δD_{VSMOW} feature is also seen in gases from the Julia field (below).

The Julia field has two gas samples that overlap with reservoir temperature (106-115°C), while two samples are very hot with temperatures of 162°C and 180°C. Similarly to the Hoover-Diana field, the Julia field's reservoir, the Wilcox formation, is a deep-water sandstone which is not conducive to the levels of organic-matter enrichment required to generate hydrocarbons. Therefore, we suggest it is most likely that the lower temperatures reflect methane generation in the oil window prior to migration of the fluids to a shallower reservoir at some time in the geologic past (Figure 7). This reservoir has then subsequently been buried to the present day depth at a temperature that overlaps with the initial generation temperature of the hydrocarbons. The hot, >150°C, temperatures are not consistent with molecular based maturity estimates from the associated oils or with a previous study demonstrating a very early oil window maturity for fluids similar to ours in the Walker Ridge protraction area of ~0.5% Ro_{eq} (Milkov and Dzou, 2007). Unusually hot gases with very low δD_{VSMOW} values and moderate, apparently thermogenic $\delta^{13}C$ values have been seen before in methane from the Eagle Ford Formation and the Bakken Shale as well as various other settings (Douglas et al., 2017; Douglas et al., 2016; Shuai et al., 2018a; Wang et al., 2015). We propose four possible explanations for the anomalously hot methane temperatures. Firstly, high clumped isotope temperatures may be the result of secondary isotope effects related to methane transport. Gas diffusion, in particular, is predicted to decrease Δ_{18} values in the residual gas. For example, a diffusive loss of 30% of the methane in a reservoir, assuming inter diffusion in gas of moderate molecular weight, would cause the residual methane Δ_{18} to decrease by 0.6‰ (equivalent to about a 30°C change in temperature at temperatures of ~150°C) and δD_{VSMOW} and $\delta^{13}C_{VPDB}$ to increase by 6‰ (Douglas et al., 2017). Since the δD_{VSMOW} is significantly depleted while the $\delta^{13}C_{VPDB}$ is within the range of typical thermogenic methane samples we think that it is unlikely that diffusion processes can explain the signal we observe.

Secondly, high Δ_{18}-based apparent temperatures could represent true formation temperatures for methane originating at greater depths than is currently predicted by models of oil and gas generation (Seewald, 2003). However, the C_2–C_5 gases of these hotter gases are significantly depleted in carbon and hydrogen isotopes relative to typical oil-dissolved gases in the Gulf of Mexico. Estimates of maturity based on the $\delta^{13}C_{VPDB}$ of C_2 and C_3 would suggest a 0.2-0.5% Ro_{eq} (Whiticar, 1994) which is consistent with immature to early oil maturity. Given how isotopically light the gases are in molecular-average $\delta^{13}C$ and δD, it is unlikely that methane (and other light hydrocarbons) generated from high maturity sources deeper in the sedimentary section has migrated into the reservoir.

Thirdly, high temperature cracking experiments have produced methane with Δ_{18}-based apparent temperatures that are significantly higher than the experimental temperature (Shuai et al., 2018a). These data suggest that thermogenic cracking of sedimentary organic matter can produce methane with non-equilibrium Δ_{18} values under certain circumstances, and the high apparent temperatures that we observe may be a result of this or a similar non-equilibrium isotope effect.

Fourthly, the signature of high Δ_{18}-temperatures could be produced by a similar mechanism as seen in recent laboratory alkane cracking experiments (Dong et al 2019) and unconventional associated gases (Xie et al 2019). These studies indicate that methane is initially produced with a strong depletion in $\Delta^{12}CH_2D_2$ but an equilibrium $\Delta^{13}CH_3D$ signature, creating an artificially high Δ_{18}-temperature. As the reaction progresses, the $\Delta^{12}CH_2D_2$ increases to values closer to equilibrium values, while the $\Delta^{13}CH_3D$ remains unchanged. The primary cause of this anomaly is a combinatorial isotope effect associated with the combination of a relatively high D/H methyl pool and a relatively low D/H abstracted or radical hydrogen atom pool.

6. CONCLUSIONS

We have presented a survey of isotopic composition ($\delta^{13}C_{VPDB}$, δD_{VSMOW} and Δ_{18}, $\Delta^{13}CH_3D$ and $\Delta^{12}CH_2D_2$ clumped isotope indices) of C_1-C_5 hydrocarbon gases and maturity estimates from a suite of diverse petroleum systems in the Gulf of Mexico (Figure 8). Our analysis indicates a diverse set of origins including moderate and high maturity thermogenic methane formed in equilibrium with respect to clumped isotope indices, low maturity thermogenic methane formed out of equilibrium (for any of several suggested reasons), and microbial gas. Methane in gas and oil reservoirs of the Galveston 209 field exhibits apparent temperatures that are consistent with oil-window to gas-window maturity. The methane clumped isotope apparent temperatures that represent the thermogenic endmembers among gases in the Hoover-Diana, Julia, and Genesis fields (101 - 118ºC) are consistent with early to main-stage oil window maturity, as also suggested by constraints provided by molecular geochemistry of associated oils. In the Julia field, we find very low δD_{VSMOW} gases with clumped isotope temperatures that yield formation temperatures higher than expected (> 160ºC) given other independent constraints. This signature has been seen in other petroleum systems including the Eagle Ford and the Bakken shales. We hypothesize that this signature is likely due to a previously seen kinetic isotope effect that occurs during early catagenic processes (Shuai et al., 2018a; Dong et al., 2019; Xie et al., 2019). We investigate the Δ_{18} endmember of microbial methane and find that in the Hadrian field, the Hoover-Diana fields and the Pleistocene gases of the Genesis field, the microbial Δ_{18} endmember is consistent with the present-day reservoir temperature, implying that methanogenesis is producing secondary microbial methane from the biodegradation of oil in equilibrium with the *in situ* temperature. In the Pliocene reservoir of the

Genesis field, we find that the microbial endmember is several per mil more enriched than the expected Δ_{18} of methane produced in equilibrium with the well temperature. This scenario is consistent with microbial methane forming at shallower depths, possibly through the biodegradation of an early oil charge, and being transported to greater depths as a result of post generation burial. This observation has important implications because, when integrated with an understanding of the thermal history of the reservoir interval of interest, one is finally able to constrain the time in the geologic past that oils migrated into the reservoir using Δ_{18}-temperatures. Additionally we show that although in laboratory settings, microbial methane can be produced at temperatures up to 105^{o}C (Brock, 1985), in the Gulf of Mexico, microbial methane is dominantly produced below ~60^{o}C.

ACKNOWLEDGEMENTS:
Thanks to Max Lloyd and Peter Douglas for help with clumped isotope measurements. This work was financed and sponsored by ExxonMobil Upstream Research Company.

REFERENCES CITED

Ash J. L., Egger M., Treude T., Kohl I., Cragg B., Parkes R. J., Slomp C. P., Sherwood Lollar B. and Young E. D. (2019) Exchange catalysis during anaerobic methanotrophy revealed by 12CH2D2 and 13CH3D in methane. *Geochemical Perspectives Letters* **10**, 26–30.

Barry P. H., Lawson M., Meurer W. P., Cheng A. and Ballentine C. J. (2018) Noble Gases in Deepwater Oils of the U.S. Gulf of Mexico. *Geochemistry, Geophysics, Geosystems* **19**, 4218–4235.

Bernard B. B., Brooks J. M. and Sackett W. M. (1978) Light hydrocarbons in recent Texas continental shelf and slope sediments. *Journal of Geophysical Research: Oceans* **83**, 4053–4061.

Brock T. D. (1985) Life at High Temperatures. *Science* **230**, 132–138.

Chung H. M., Gormly J. R. and Squires R. M. (1988) Origin of gaseous hydrocarbons in subsurface environments: Theoretical considerations of carbon isotope distribution. *Chemical Geology* **71**, 97–104.

Connan J. (1984) Biodegradation of crude oils in reservoirs. In *Advances in Petroleum Geochemistry* (ed. J. and W. Brooks D. H. ,.). Academic Press, London.

Dong G., Xie H., Formolo M., Lawson M., Sessions A. and Eiler J. (2019) Methane Clumped Isotope Constraints on the Equilibrium and Kinetics of Unconventional Gases. In *Goldschmidt Abstracts* Goldschmidt. Barcelona.

Douglas P. M. J., Stolper D. A., Eiler J. M., Sessions A. L., Lawson M., Shuai Y., Bishop A., Podlaha O. G., Ferreira A. A., Santos Neto E. V., Niemann M., Steen A. S., Huang L., Chimiak L., Valentine D. L., Fiebig J., Luhmann A. J., Seyfried W. E., Etiope G., Schoell

M., Inskeep W. P., Moran J. J. and Kitchen N. (2017) Methane clumped isotopes: Progress and potential for a new isotopic tracer. *Organic Geochemistry* **113**, 262–282.

Douglas P. M. J., Stolper D. A., Smith D. A., Walter Anthony K. M., Paull C. K., Dallimore S., Wik M., Crill P. M., Winterdahl M., Eiler J. M. and Sessions A. L. (2016) Diverse origins of Arctic and Subarctic methane point source emissions identified with multiply-substituted isotopologues. *Geochimica et Cosmochimica Acta* **188**, 163–188.

Etiope G. and Sherwood Lollar B. (2013) ABIOTIC METHANE ON EARTH. *Reviews of Geophysics* **51**, 276–299.

Forrest J. Marcucci, E. ,. Scott, P. (2005) Geothermal Gradients and Subsurface Temperatures in the Northern Gulf of Mexico. *GCAGS Transactions* **55**, 233–248.

Franks S. G. and Uchytil S. J. (2016) Geochemistry of formation waters from the subsalt Tubular Bells Field, offshore Gulf of Mexico: Implications for fluid movement and reservoir continuity. *AAPG Bulletin* **100**, 943–967.

Galloway W. E. Ganey-Curry, P. E. ,. Li, X. ,. Buffler, R. T. (2000) Cenozoic depositional history of the Gulf of Mexico basin. *AAPG Bulletin* **84**, 1743–1774.

Gilg H. A. and Sheppard S. M. F. (1996) Hydrogen isotope fractionation between kaolinite and water revisited. *Geochimica et Cosmochimica Acta* **60**, 529–533.

Giunta T., Young E. D., Warr O., Kohl I., Ash J. L., Martini A., Mundle S. O. C., Rumble D., Pérez-Rodríguez I., Wasley M., LaRowe D. E., Gilbert A. and Sherwood Lollar B. (2019) Methane sources and sinks in continental sedimentary systems: New insights from paired clumped isotopologues 13CH3D and 12CH2D2. *Geochimica et Cosmochimica Acta* **245**, 327–351.

Gruen D. S., Wang D. T., Könneke M., Topçuoğlu B. D., Stewart L. C., Goldhammer T., Holden J. F., Hinrichs K.-U. and Ono S. (2018) Experimental investigation on the controls of clumped isotopologue and hydrogen isotope ratios in microbial methane. *Geochimica et Cosmochimica Acta* **237**, 339–356.

Hood K. C. Wenger, L. M. ,. Gross, O. P. ,. Harrison, S. C. (2002) Hydrocarbon systems analysis of the northern Gulf of Mexico: Delineation of hydrocarbon migration patways using seeps and seismic imaging. In *Surface exploration case histories: Applications of geochemistry, magnetics and remote sensing* (ed. D. and L. Schumacher L. A.). AAPG Studies in Geology and SEG Geophysical References Series. pp. 25–40.

Horibe Y. and Craig H. (1995) DH fractionation in the system methane-hydrogen-water. *Geochimica et Cosmochimica Acta* **59**, 5209–5217.

Hunt J. M. (1995) *Petroleum Geochemistry and Geology*., Freeman, New York.

Inagaki F., Hinrichs K.-U., Kubo Y., Bowles M. W., Heuer V. B., Hong W.-L., Hoshino T., Ijiri A., Imachi H., Ito M., Kaneko M., Lever M. A., Lin Y.-S., Methé B. A., Morita S.,

Morono Y., Tanikawa W., Bihan M., Bowden S. A., Elvert M., Glombitza C., Gross D., Harrington G. J., Hori T., Li K., Limmer D., Liu C.-H., Murayama M., Ohkouchi N., Ono S., Park Y.-S., Phillips S. C., Prieto-Mollar X., Purkey M., Riedinger N., Sanada Y., Sauvage J., Snyder G., Susilawati R., Takano Y., Tasumi E., Terada T., Tomaru H., Trembath-Reichert E., Wang D. T. and Yamada Y. (2015) Exploring deep microbial life in coal-bearing sediment down to ~2.5 km below the ocean floor. *Science* **349**, 420–424.

Martini A. M., Budai J. M., Walter L. M. and Schoell M. (1996) Microbial generation of economic accumulations of methane within a shallow organic-rich shale. *Nature* **383**, 155–158.

Milkov A. V. and Dzou L. (2007) Geochemical evidence of secondary microbial methane from very slight biodegradation of undersaturated oils in a deep hot reservoir. *Geology* **35**, 455–458.

Ni Y., Ma Q., Ellis G. S., Dai J., Katz B., Zhang S. and Tang Y. (2011) Fundamental studies on kinetic isotope effect (KIE) of hydrogen isotope fractionation in natural gas systems. *Geochimica et Cosmochimica Acta* **75**, 2696–2707.

Nunn J. A. Sassen, R. (1986) The Framework of Hydrocarbon Generation and Migration, Gulf of Mexico Continental Slope. *Transactions-Gulf Coast Association of Geological Societies* **36**.

Ono S., Wang D. T., Gruen D. S., Sherwood Lollar B., Zahniser M. S., McManus B. J. and Nelson D. D. (2014) Measurement of a Doubly Substituted Methane Isotopologue, 13CH3D, by Tunable Infrared Laser Direct Absorption Spectroscopy. *Analytical Chemistry* **86**, 6487–6494.

Peters K. E. Walters, C. C. ,. Moldowan, J. M. (2005) *The Biomarker Guide, Volume 2: Biomarkers and isotopes in petroleum exploration and Earth History*., Cambridge University Press, Cambridge, UK.

Peterson B. K., Formolo M. J. and Lawson M. (2018) Molecular and detailed isotopic structures of petroleum: Kinetic Monte Carlo analysis of alkane cracking. *Geochimica et Cosmochimica Acta* **243**, 169–185.

Radke M., Welte D. H. and Willsch H. (1986) Maturity parameters based on aromatic hydrocarbons: Influence of the organic matter type. *Organic Geochemistry* **10**, 51–63.

Rice D. D. Claypool, G. E. (1981) Generation, Accumulation and Resource Potential of Biogenic Gas. *AAPG Bulletin* **65**, 5–25.

Rooney M. A., Claypool G. E. and Moses Chung H. (1995) Modeling thermogenic gas generation using carbon isotope ratios of natural gas hydrocarbons. *Chemical Geology* **126**, 219–232.

Rowan M. G. Weimer, P. (1998) Salt-sediment interaction, north Green Canyon and Ewing Bank (offshore Louisiana) northern Gulf of Mexico. In AAPG Bulletin. pp. 1055–1082.

Sassen R., Joye S., Sweet S. T., DeFreitas D. A., Milkov A. V. and MacDonald I. R. (1999) Thermogenic gas hydrates and hydrocarbon gases in complex chemosynthetic communities, Gulf of Mexico continental slope. *Organic Geochemistry* **30**, 485–497.

Sassen R., Milkov A. V., Ozgul E., Roberts H. H., Hunt J. L., Beeunas M. A., Chanton J. P., DeFreitas D. A. and Sweet S. T. (2003) Gas venting and subsurface charge in the Green Canyon area, Gulf of Mexico continental slope: evidence of a deep bacterial methane source? *Organic Geochemistry* **34**, 1455–1464.

Schoell M. (1980) The hydrogen and carbon isotopic composition of methane from natural gases of various origins. *Geochimica et Cosmochimica Acta* **44**, 649–661.

Seewald J. S. (2003) Organic-Inorganic interactions in petroleum-producing sedimentary basins. *Nature* **426**. Available at: https://doi.org/10.1038/nature02132.

Shuai Y., Douglas P. M. J., Zhang S., Stolper D. A., Ellis G. S., Lawson M., Lewan M. D., Formolo M., Mi J., He K., Hu G. and Eiler J. M. (2018a) Equilibrium and non-equilibrium controls on the abundances of clumped isotopologues of methane during thermogenic formation in laboratory experiments: Implications for the chemistry of pyrolysis and the origins of natural gases. *Geochimica et Cosmochimica Acta* **223**, 159–174.

Shuai Y., Etiope G., Zhang S., Douglas P. M. J., Huang L. and Eiler J. M. (2018b) Methane clumped isotopes in the Songliao Basin (China): New insights into abiotic vs. biotic hydrocarbon formation. *Earth and Planetary Science Letters* **482**, 213–221.

Stolper D. A., Lawson M., Formolo M. J., Davis C. L., Douglas P. M. J. and Eiler J. M. (2017) The utility of methane clumped isotopes to constrain the origins of methane in natural gas accumulations. *Geological Society, London, Special Publications* **468**. Available at: http://sp.lyellcollection.org/content/early/2017/12/12/SP468.3.abstract.

Stolper D. A., Martini A. M., Clog M., Douglas P. M., Shusta S. S., Valentine D. L., Sessions A. L. and Eiler J. M. (2015) Distinguishing and understanding thermogenic and biogenic sources of methane using multiply substituted isotopologues. *Geochimica et Cosmochimica Acta* **161**, 219–247.

Stolper D. A., Sessions A. L., Ferreira A. A., Santos Neto E. V., Schimmelmann A., Shusta S. S., Valentine D. L. and Eiler J. M. (2014) Combined 13C–D and D–D clumping in methane: Methods and preliminary results. *Geochimica et Cosmochimica Acta* **126**, 169–191.

Stolper, Lawson M., Davis C. L., Ferreira A. A., Neto E. V. S., Ellis G. S., Lewan M. D., Martini A. M., Tang Y., Schoell M., Sessions A. L. and Eiler J. M. (2014) Formation temperatures of thermogenic and biogenic methane. *Science* **344**, 1500–1503.

Sullivan M. and T. P. (2002) Characterization of fine-grained deep-water turbidite reservoirs: examples from the Diana sub-basin, western, Gulf of Mexico. In *Deep-water core workshop, Northern Gulf of Mexico. Gulf Coast Section* (ed. M. S. Paul Weimer Morgan

Sullivan, John Kendrick, David Pyles and Art Donovan). Society for Sedimentary Geology.

Sullivan M. and Templet P. (2002) Characterization of fine-grained deep-water turbidite reservoirs: examples from the Diana sub-basin, western Gulf of Mexico. In Deep-water core workshop. Northern Gulf of Mexico. Gulf Coast Section. SEPM Publication.

Sweeney J. and B. Alan (1990) Evaluation of a simple Model of Vitrinite Reflectance based on Chemical Kinetics. *AAPG Bulletin* **74**.

Sweet M. L. and S. L. T. (2007) Genesis field, Gulf of Mexico: Recognizing reservoir compartments on geologic and production times cales in the deep-water reservoirs. *AAPG Bull.* **91**, 1701–1729.

Tang Y., Perry J. K., Jenden P. D. and Schoell M. (2000) Mathematical modeling of stable carbon isotope ratios in natural gases†. *Geochimica et Cosmochimica Acta* **64**, 2673–2687.

Tissot B. P. and D. W. (1984) *Petroleum Formation and occurence.*, Springer Verlag, Berlin.

USEIA (2016) *U.S. Crude Oil and Natural Gas Proved Reserves, Year-end 2016.*, Washington, DC.

Valentine D. L., Chidthaisong A., Rice A., Reeburgh W. S. and Tyler S. C. (2004) Carbon and hydrogen isotope fractionation by moderately thermophilic methanogens11Associate editor: N. E. Ostrom. *Geochimica et Cosmochimica Acta* **68**, 1571–1590.

Wang D. T., Gruen D. S., Lollar B. S., Hinrichs K.-U., Stewart L. C., Holden J. F., Hristov A. N., Pohlman J. W., Morrill P. L., Könneke M., Delwiche K. B., Reeves E. P., Sutcliffe C. N., Ritter D. J., Seewald J. S., McIntosh J. C., Hemond H. F., Kubo M. D., Cardace D., Hoehler T. M. and Ono S. (2015) Nonequilibrium clumped isotope signals in microbial methane. *Science* **348**, 428–431.

Wang Y., Sessions A. L., Nielsen R. J. and Goddard Iii W. A. (2009a) Equilibrium 2H/1H fractionations in organic molecules: I. Experimental calibration of ab initio calculations. *Geochimica et Cosmochimica Acta* **73**, 7060–7075.

Wang Y., Sessions A. L., Nielsen R. J. and Goddard W. A. (2009b) Equilibrium 2H/1H fractionations in organic molecules. II: Linear alkanes, alkenes, ketones, carboxylic acids, esters, alcohols and ethers. *Geochimica et Cosmochimica Acta* **73**, 7076–7086.

Whiticar M. J. (1999) Carbon and hydrogen isotope systematics of bacterial formation and oxidation of methane. *Chemical Geology* **161**, 291–314.

Whiticar M. J. (1994) Correlation of Natural Gases with their Sources. In *The Petroleum System-From Source to Trap* AAPG Special Volume.

Xie H., Formolo M. J., Lawson M. and Eiler J. (2019) Formation mechanisms of thermogenic methane revealed from 13CH3D and 12CH2D2 measurements. In International Clumped Isotope Workshop. Long Beach, CA USA.

Young E. D., Kohl I. E., Lollar B. S., Etiope G., Rumble D., Li S., Haghnegahdar M. A., Schauble E. A., McCain K. A., Foustoukos D. I., Sutclife C., Warr O., Ballentine C. J., Onstott T. C., Hosgormez H., Neubeck A., Marques J. M., Pérez-Rodríguez I., Rowe A. R., LaRowe D. E., Magnabosco C., Yeung L. Y., Ash J. L. and Bryndzia L. T. (2017) The relative abundances of resolved l2CH2D2 and 13CH3D and mechanisms controlling isotopic bond ordering in abiotic and biotic methane gases. *Geochimica et Cosmochimica Acta* **203**, 235–264.

FIGURE CAPTIONS

Figure 1. Map of the sample Locations in the Gulf of Mexico.

Figure 2. HR scan of methane and adducted methane peaks at mass 18 using the H4 CDD collector. From left to right: $^{13}CH_3D$, $^{13}CH_5$, $^{12}CH_2D_2$, $^{12}CH_4D$.

Figure 3. Chung plots of δD_{VSMOW} and $\delta^{13}C_{VPDB}$ for C1-C5 hydrocarbons. The Chung method is used to estimate the relative contribution of microbial methane. N refers to the number of carbons in a hydrocarbon molecule. Therefore, when plotting 1/n, '1' refers to methane, '0.5' refers to ethane, etc.

Figure 4. Methane δD_{VSMOW} and $\delta^{13}C_{VPDB}$ overlaid on source fields derived from (Whiticar, 1999).

Figure 5. Scatter plot of Galveston, Genesis, Hoover-Diana, Hadrian and Julia data of (A) δD_{VSMOW} vs $\delta^{13}C_{VPDB}$, (B) (C_1/C_2+C_3) vs $\delta^{13}C_{VPDB}$, (C) Δ_{18}–Temperature vs $\delta^{13}C$, (D) Δ_{18}–Temperature vs δD_{VSMOW}, and (E) $\delta^{13}C_{VPDB}$ vs Δ_{18}–Temperature-Reservoir Temperature.

Figure 6. Scatter plot of Galveston, Hoover-Diana and Hadrian data of $\Delta^{12}CH_2D_2$ vs $\Delta^{13}CH_3D$ with equilibrium indicated in a blue line with blue squares plotted in 100°C increments.

Figure 7. Scatter plot of Hoover-Diana data (A) δD_{VSMOW} vs $\delta^{13}C_{VPDB}$, (B) Δ_{18}–Temperature vs $\delta^{13}C$, (C) Δ_{18}–Temperature vs δD_{VSMOW}. The green line is the mixing model for Hoover-Diana that is described in the text.

Figure 8. Summary figure of the main findings of the text. The samples that have been identified as microbial, thermogenic and displaying a kinetic isotope effect are depicted for each reservoir.

Supplementary Information:

Figure S1a

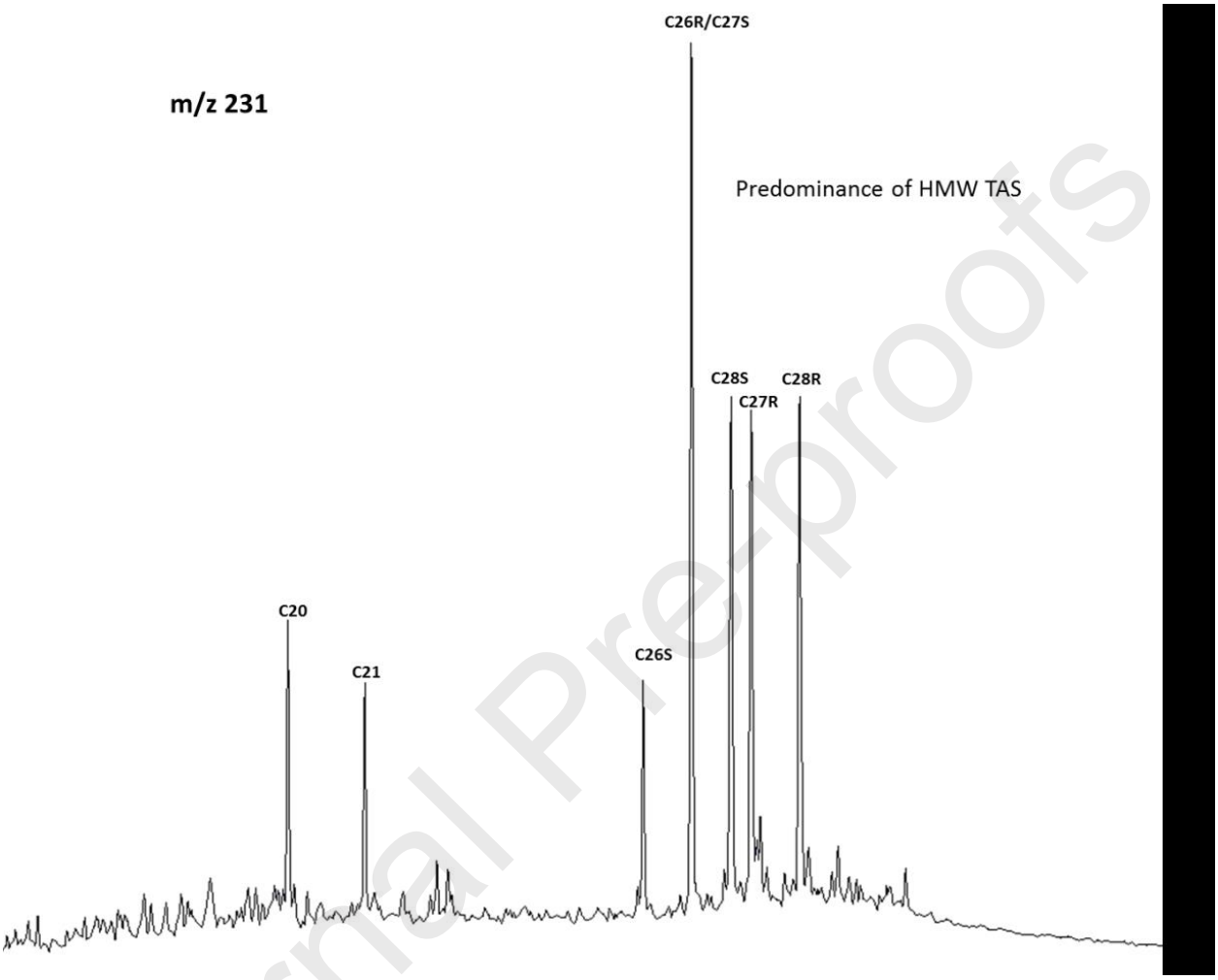

Figure S1b

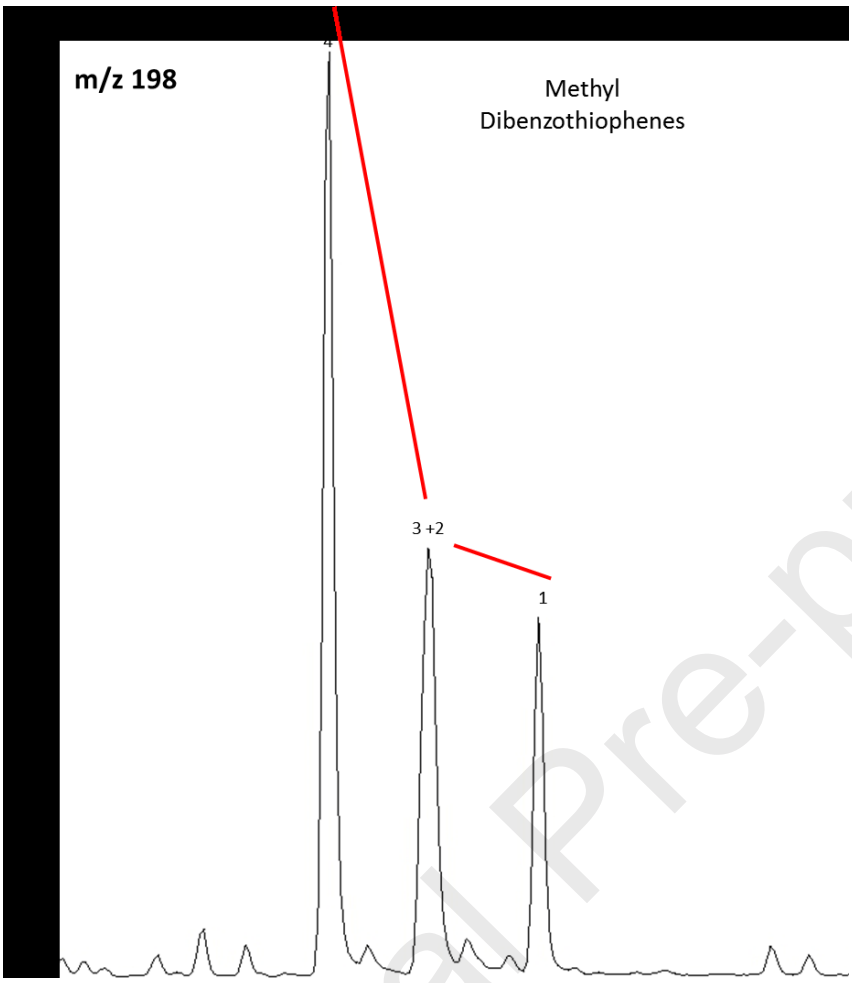

Figure S1: Aromatic GC/MS m/z 231 (a) and 198 (b)of oil from a representative Genesis oil provide independent constraints on the thermal maturity of these fluids. Elevated 4MDBT to 3+2MDBT and 3+2MDBT greater than 1MDBT, and a 4MDBT to 1MDT ratio, sometimes referred to as the MDR ratio, are consistent with main stage oil window maturity (Radke et al., 1986) . Similarly, a predominance of high molecular weight tri-aromatic steroids to low molecular weight tri-aromatic steroids (Peters, 2005) suggest main stage oil window maturity (> 0.8% $R_o$eq).

Figure S2

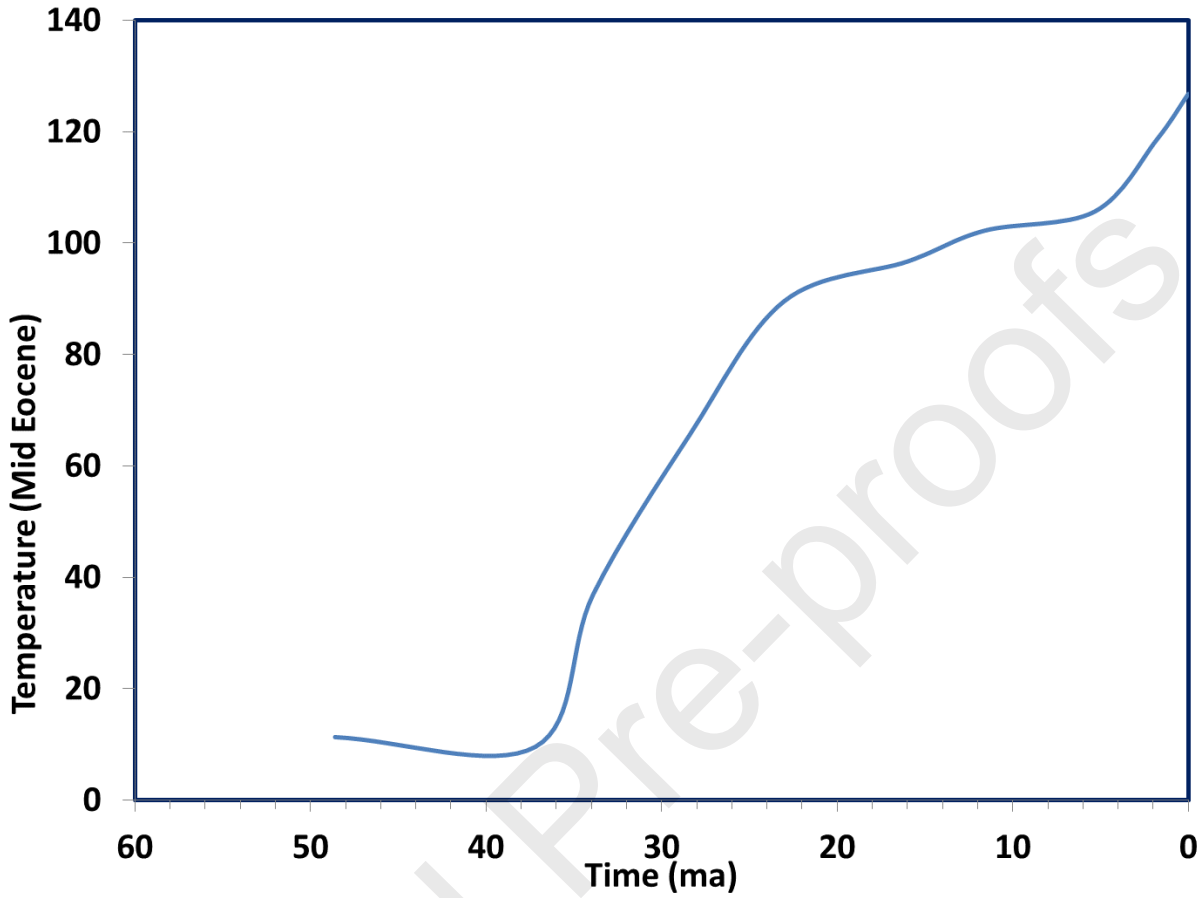

Figure S2: An off-structure 1-D basin model constructed in the vicinity of the Hoover-Diana fields was developed to place constraints on the thermal history of the Eocene (given as the mid-Eocene) source in this region. This model incorporates a Jurassic rifting event that results in a thermal anomaly that peaks at 95 mW/m^2 at 160 Ma and decays to a steady state basal heat flow of 44 mW/m^2 present day. Sedimentation rate in the mini basin was fairly constant from the Jurassic through to the end of the Miocene (10 – 150 m/myr). The sedimentation rate increased significantly in the Pliocene (~200 m/myr) and the Pleistocene (~1150 m/myr) as shelf edge progradation in the northwestern Gulf of Mexico was fed by transport and deposition of significant volumes of sediment from the Central Mississippi embayment and to a lesser extent the Rio Grande Delta (Galloway, 2000). The model predicts a present day temperature for a Middle Eocene source of 127^{o}C.

Figure 1

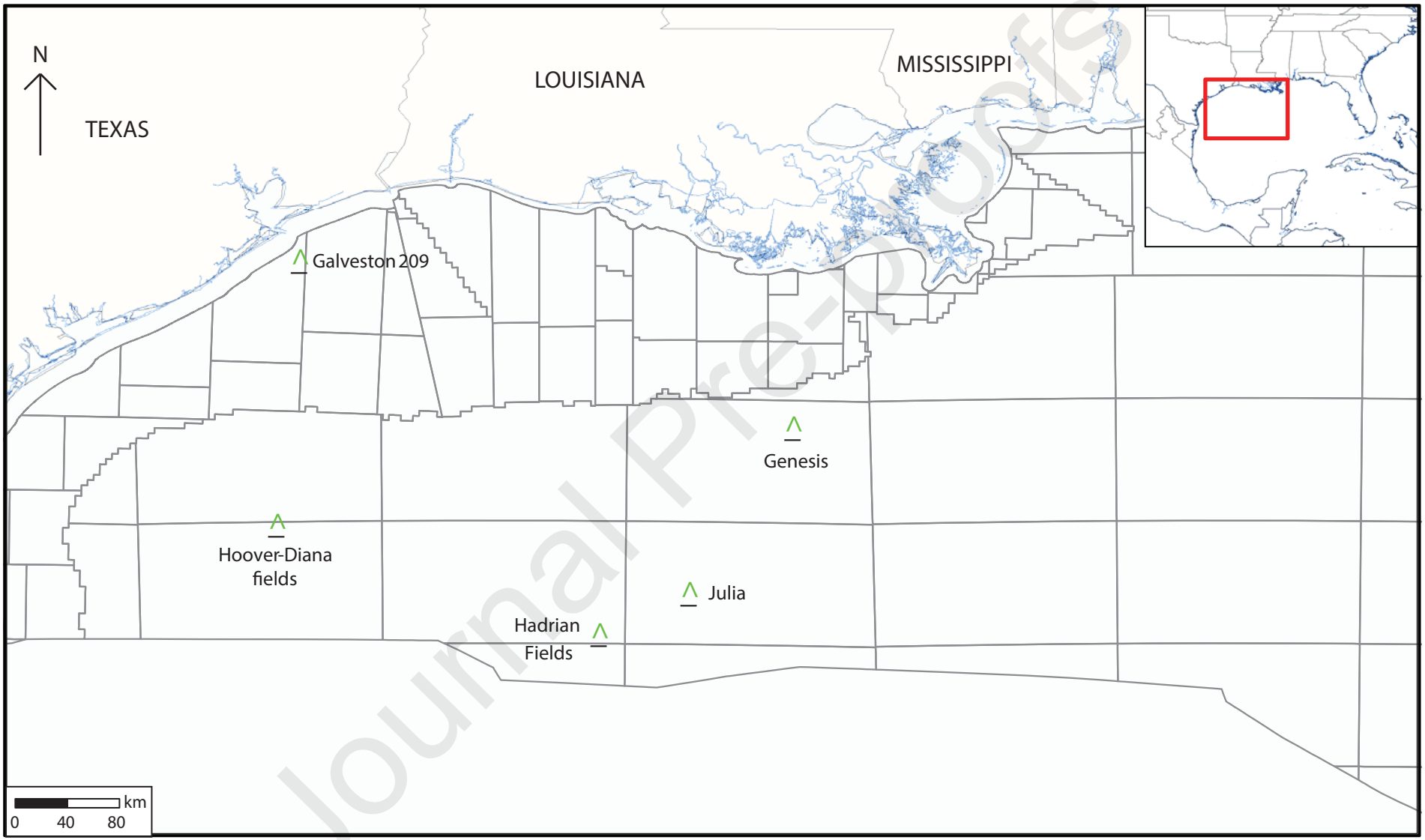

Figure 2

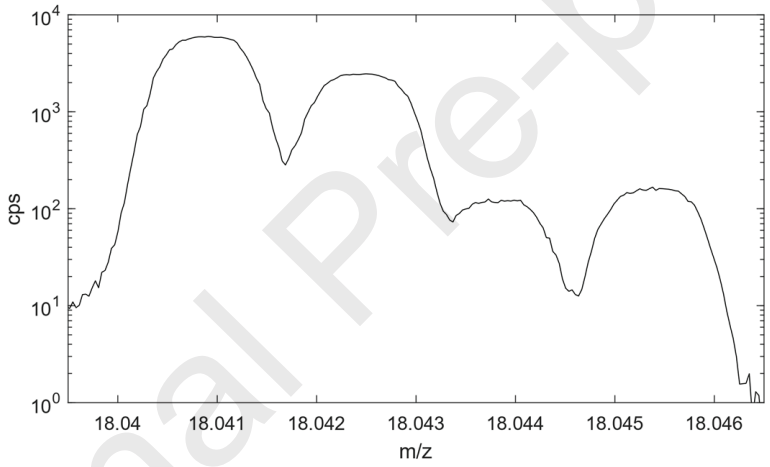

Figure 3

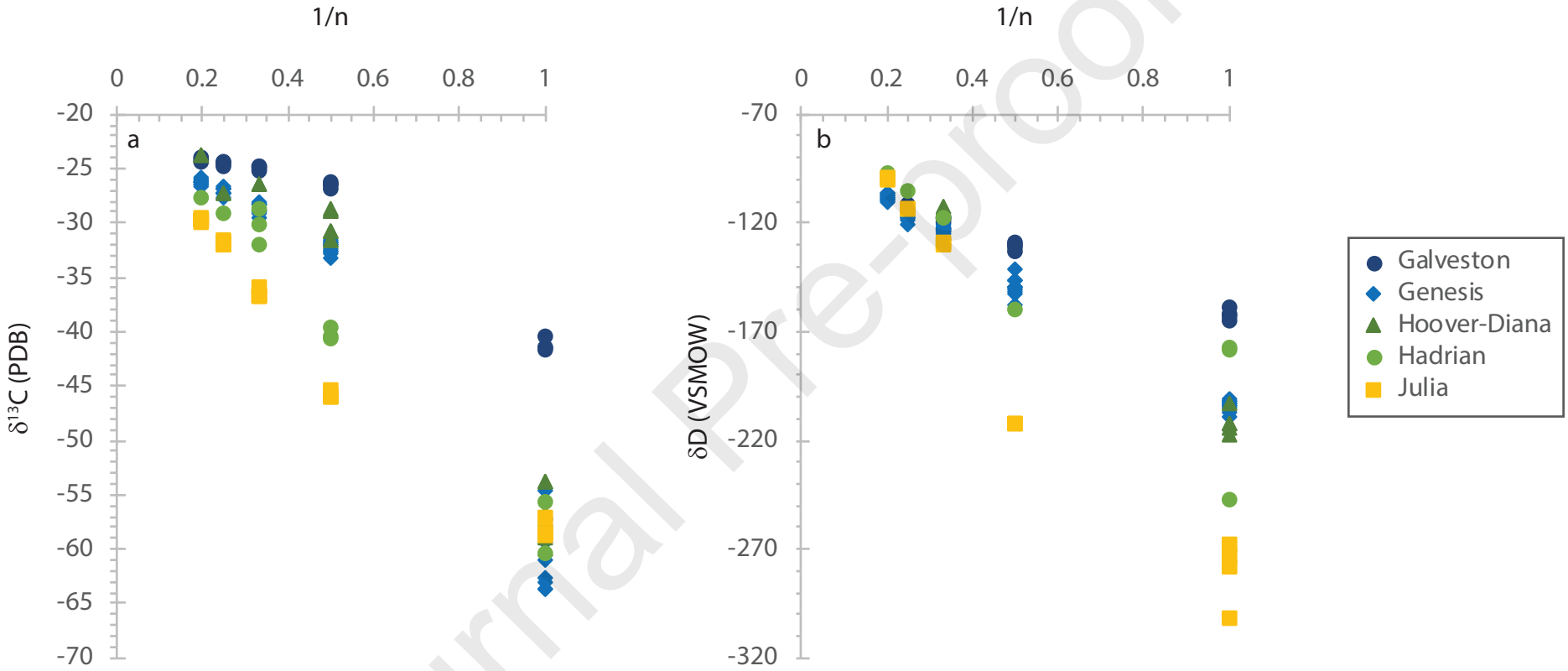

Figure 4

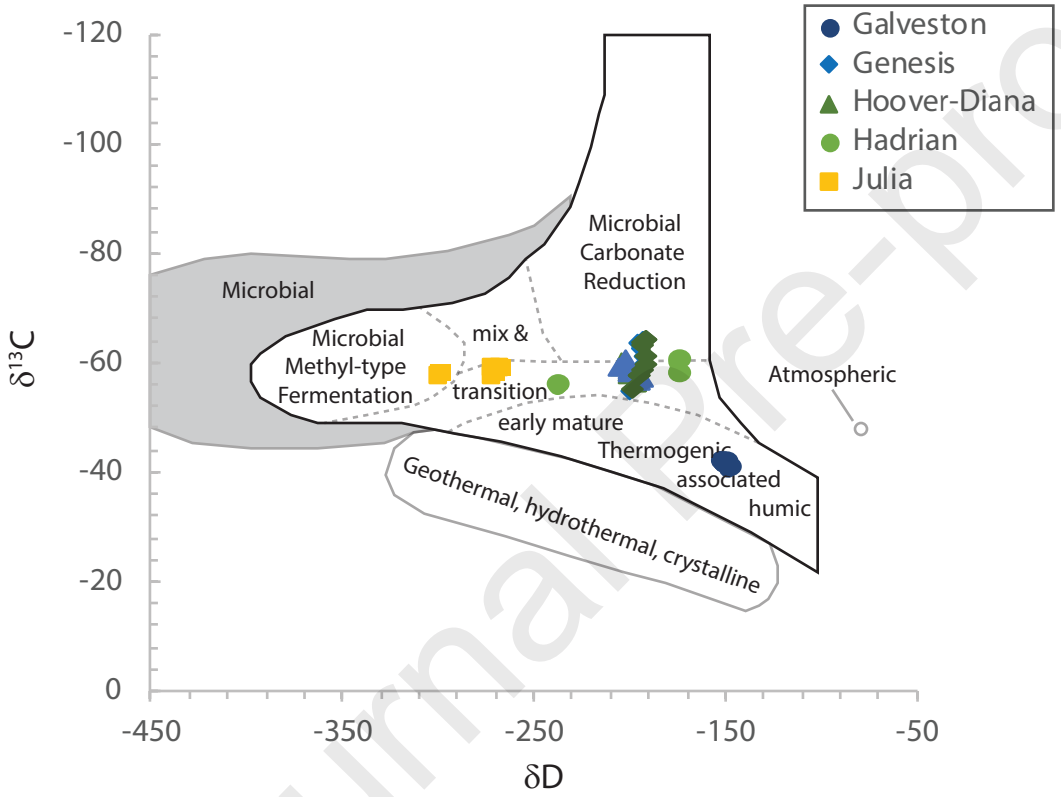

Figure 5

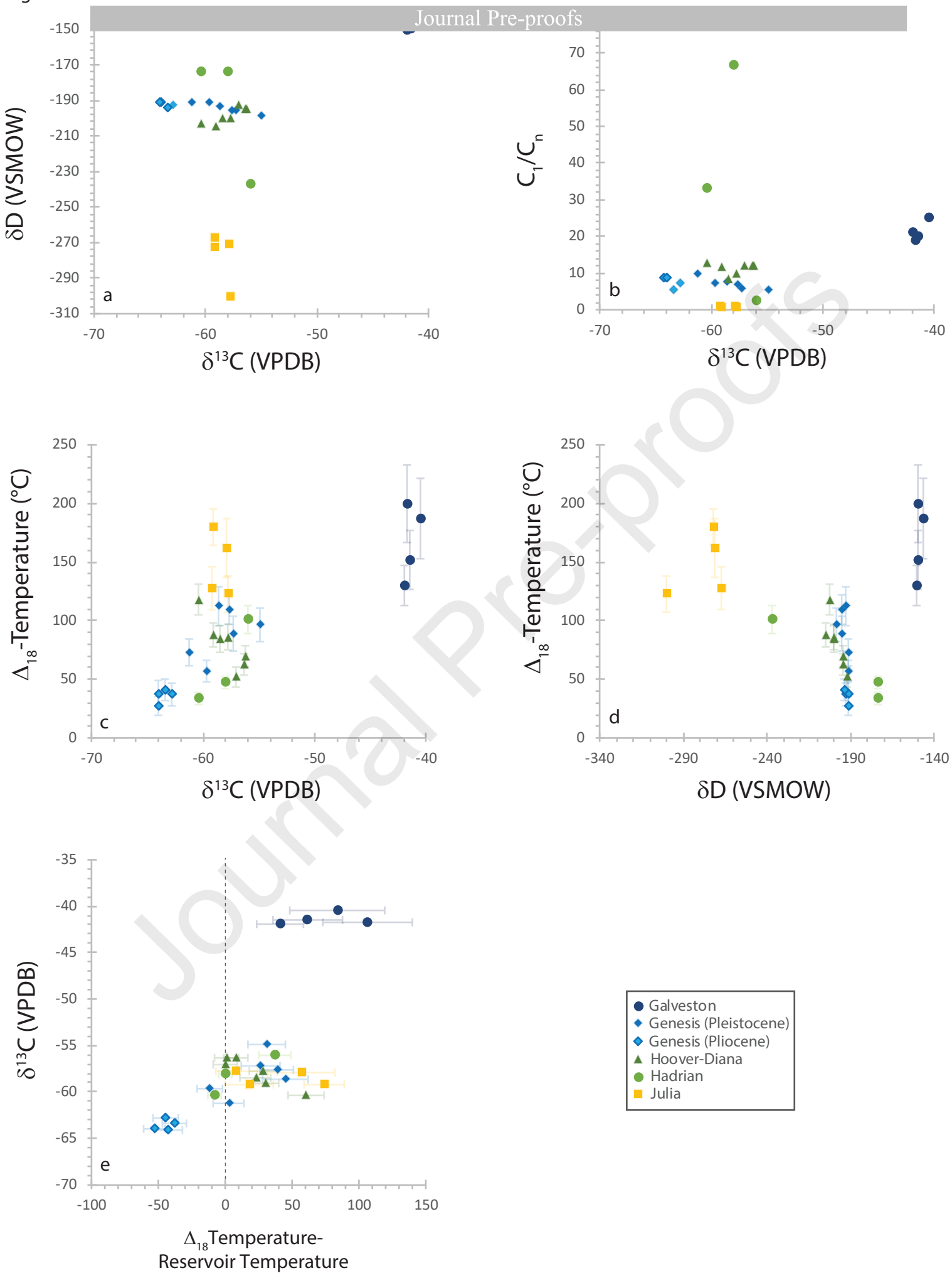

Figure 6

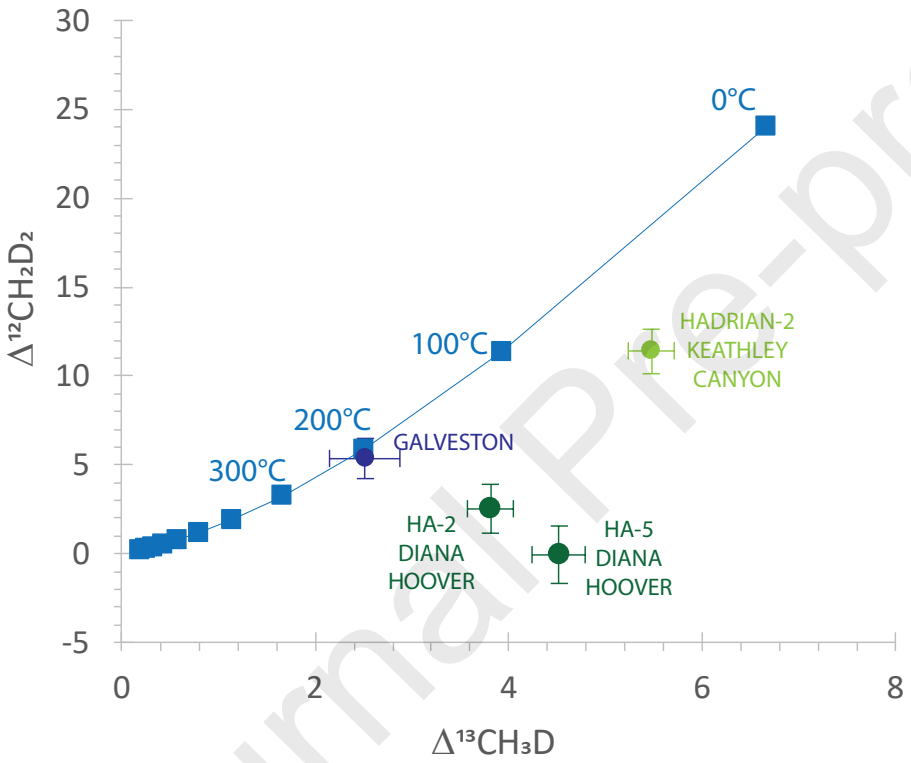

Figure 7

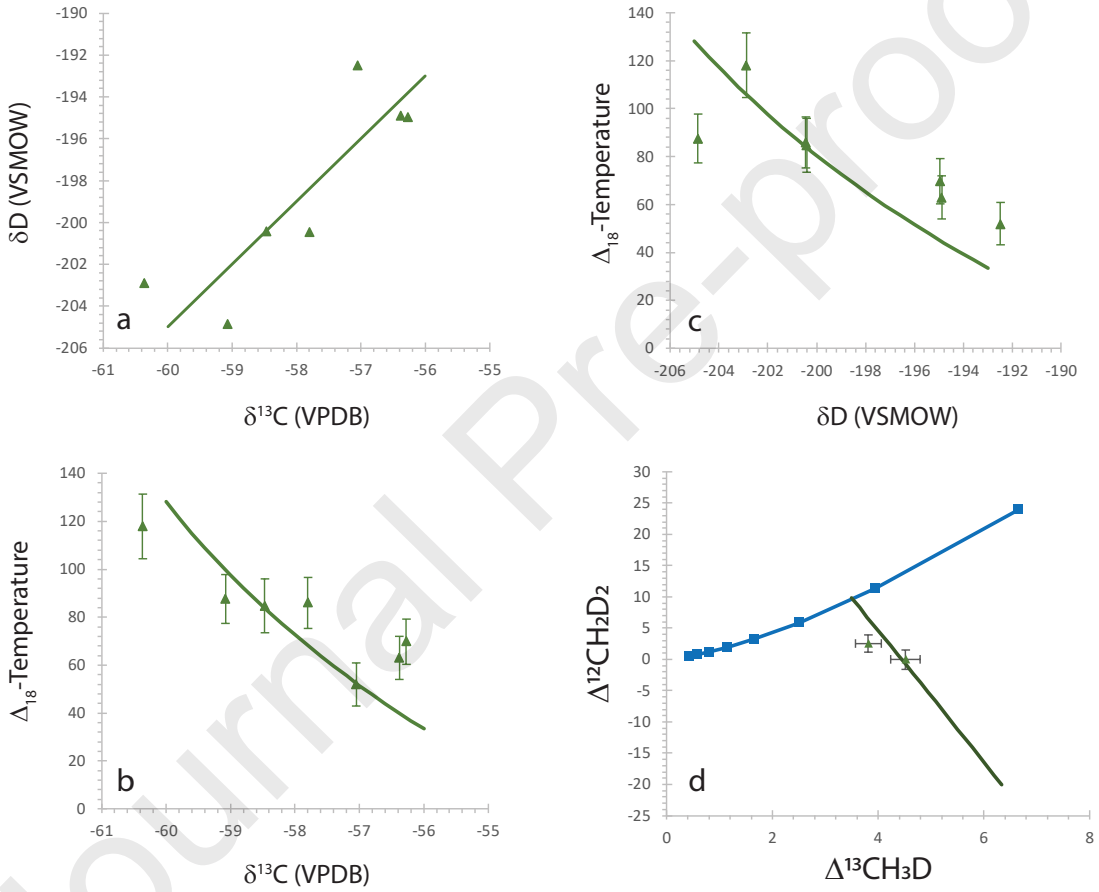

Figure 8

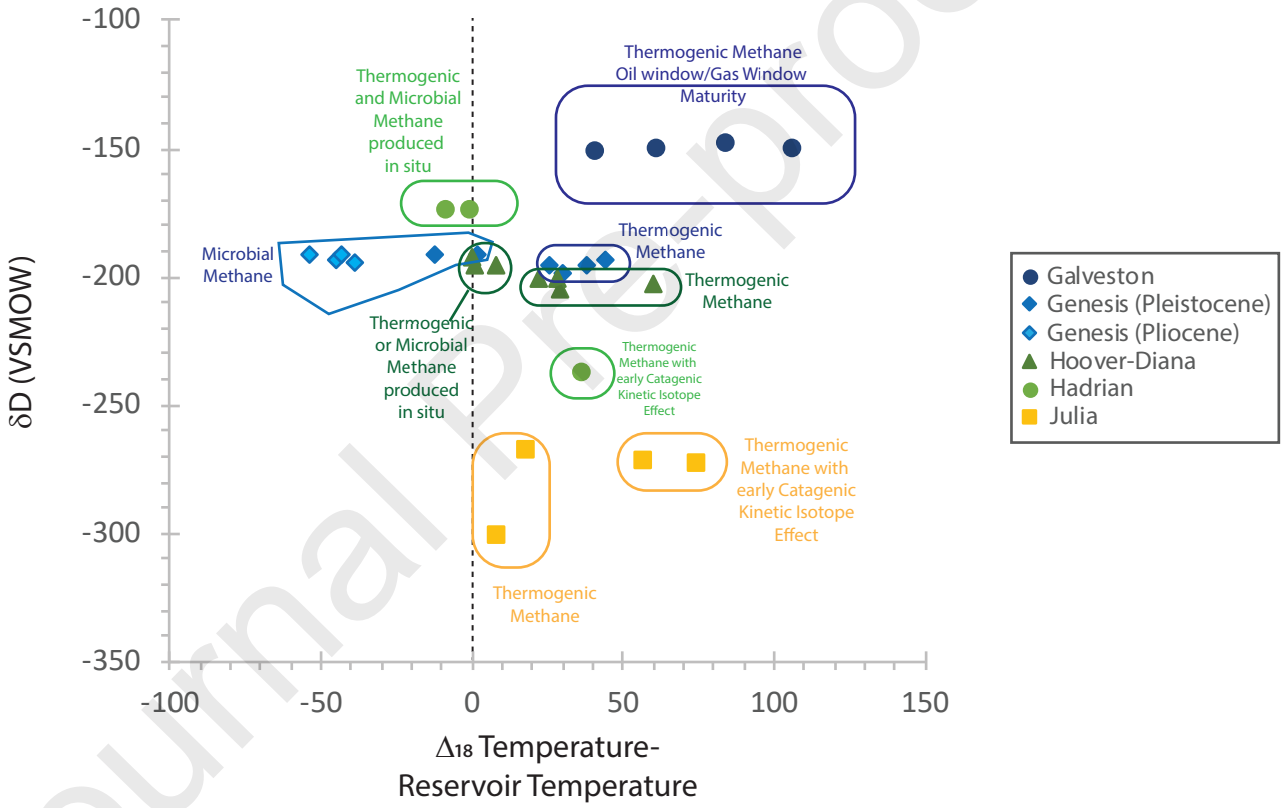

Table 1-Methane Singly Substituted and Clumped Isotope ratios

Basin	Well	Field	Depth (m)	Well temperature (°C)	δD of Methane	$\delta^{13}C$ of methane	Δ_{18}	1σ Standard Error	$T(\Delta_{18})$ °C	Temperature Error	$\Delta^{13}CH_3D$	1σ Standard Error	$\Delta^{12}CH_2D_2$	1σ Standard Error
Galveston Island	A3	Galveston Island	2812	94	-149.8	-41.7	2.6	0.35	200	33	-	-	-	-
Galveston Island	B5	Galveston Island	2920	103	-147.0	-40.5	2.8	0.39	187	34	-	-	-	-
Galveston Island	B7	Galveston Island	2483	91	-149.6	-41.5	3.2	0.36	152	25	-	-	-	-
Galveston Island	B7D	Galveston Island	2483	89	-150.8	-41.9	3.6	0.27	130	17	2.51	0.37	5.36	1.15
Green Canyon	5909 A12 ST4	Genesis	4618	79	-194.0	-63.4	5.7	0.27	41	9	-	-	-	-
Green Canyon	5909 A15 ST1	Genesis	3969	66	-198.8	-55.0	4.2	0.28	96	14	-	-	-	-
Green Canyon	5909 A3	Genesis	4053	69	-191.1	-59.7	5.2	0.25	57	9	-	-	-	-
Green Canyon	5909 A7	Genesis		81	-191.4	-64.0	6.1	0.26	27	8	-	-	-	-

Green Canyon	5909 A7 (Repeat Sample)	Genesis		81	-191.1	-64.1	5.7	0.31	38	10	-	-	-	-
Green Canyon	5911 A1 ST3	Genesis	3998	71	-195.3	-57.7	4.0	0.24	109	13	-	-	-	-
Green Canyon	5911 A16	Genesis	4494	82	-192.7	-62.9	5.8	0.29	37	10	-	-	-	-
Green Canyon	5911 A2 BP1	Genesis	3886	63	-195.3	-57.3	4.4	0.32	89	15	-	-	-	-
Green Canyon	7996 A4	Genesis	3912	71	-191.2	-61.2	4.8	0.27	73	11	-	-	-	-
Green Canyon	7996 A5	Genesis	3898	68	-193.3	-58.7	3.9	0.31	112	17	-	-	-	-
Sigsby Sub Basin	HA2-sidetrack	Diana-Hoover	2593	58	-202.9	-60.4	3.8	0.24	118	13	3.81	0.24	2.53	1.40
Sigsby Sub Basin	HA5-sidetrack	Diana-Hoover	2613	58	-204.9	-59.1	4.4	0.22	88	10	4.52	0.28	-0.04	1.60
Sigsby Sub Basin	SD1	Diana-Hoover	1880	52	-192.5	-57.0	5.3	0.25	52	9	-	-	-	-
Sigsby Sub Basin	DB2 - ST4	Diana-Hoover		62	-195.0	-56.3	4.9	0.24	70	9	-	-	-	-

Sigsby Sub Basin	DB-2 Diana Hoover 75°C extraction	Diana-Hoover		62	-194.9	-56.4	5.0	0.23	63	9	-	-	-	-
Sigsby Sub Basin	HA-1 QAY-710	Diana-Hoover	2742	58	-200.5	-57.8	4.5	0.24	86	11	-	-	-	-
Sigsby Sub Basin	Madison (MP-1)	Diana-Hoover	2418	62	-200.4	-58.5	4.5	0.25	85	11	-	-	-	-
Keathley Canyon	Hadrian-6	Hadrian	2904	64	-237.0	-56.0	4.1	0.23	101	12	-	-	-	-
Keathley Canyon	Hadrian -2	Hadrian	2540	42	-173.9	-60.4	6.0	0.26	34	5	-	-	-	-
Keathley Canyon	Hadrian -2	Hadrian	2975	48	-173.7	-58.0	5.6	0.24	48	5	5.48	0.24	11.39	1.24
Walker Ridge	Julia 102 ST1	Julia	8795	106	-272.0	-59.2	2.9	0.23	180	15	-	-	-	-
Walker Ridge	Julia 102 ST1	Julia	9226	115	-300.2	-57.7	3.7	0.25	123	16	-	-	-	-
Walker Ridge	Julia 102 ST1	Julia	8795	106	-271.1	-57.9	3.1	0.33	162	25	-	-	-	-
Walker Ridge	Julia 102 ST1	Julia	8888	110	-267.3	-59.2	3.6	0.29	128	18	-	-	-	-

Table 2- Compositions and Stable Isotope compositions of C1-C5 gases

Basin	Well	Field	CH_4%	C_2H_6%	C_2H_4%	C_3H_8%	C_3H_6%	iso-C_4H_{10}%	n-C_4H_{10}%	iso-C_5H_{12}%	n-C_5H_{12}%	C6+ species%	$\delta^{13}C_{CO_2}$	$\delta^{13}C_{C_2H_6}$	$\delta D_{C_2H_6}$	$\delta^{13}C_{C_3H_8}$	$\delta D_{C_3H_8}$	$\delta^{13}C_{isoC_4H_{10}}$	$\delta D_{isoC_4H_{10}}$	$\delta^{13}C_{nC_4H_{10}}$	$\delta D_{nC_4H_{10}}$	$\delta^{13}C_{isoC_5H_{12}}$	$\delta D_{isoC_5H_{12}}$	$\delta^{13}C_{nC_5H_{12}}$	$\delta D_{nC_5H_{12}}$	$CH_4/(C_2H_6+C_3H_8)$
Galveston Island	A3	Galveston Island	94.40	3.14	NaN	0.89	NaN	0.32	0.20	0.12	0.07	0.24	-8.1	-26.9	-132.6	-25.3	-118.0	-26.2	-120.4	-24.8	-111.8	-24.3	NaN	-24.4	NaN	23.4
Galveston Island	B5	Galveston Island	95.25	2.58	NaN	0.60	NaN	0.18	0.13	0.07	0.04	0.19	-7.0	-26.3	-130.8	-24.9	-123.1	-25.5	NaN	-24.6	NaN	-24.0	NaN	NaN	NaN	30.0

Galveston Island	B7	Galveston Island	94.77	3.04	NaN	0.79	NaN	0.24	0.17	0.10	0.06	0.32	-7.0	-26.4	-1129.6	-24.8	-1119.6	-25.6	-1119.5	-24.4	NaN	-24.0	NaN	-23.9	NaN	24.8
Galveston Island	B7D	Galveston Island	94.96	2.97	NaN	0.76	NaN	0.24	0.16	0.09	0.05	0.19	-7.0	-26.5	-1128.9	-24.7	-1118.0	-25.6	-1121.4	-24.3	NaN	-24.0	NaN	-24.1	NaN	25.5
GreenCanyon	59009A7	Genesis	89.41	4.32	NaN	3.13	NaN	0.57	1.16	0.36	0.31	0.33	-222.5	-32.6	-1146.1	-28.9	-1123.6	-29.5	-1121.0	-27.2	-1115.8	-27.7	-1110.9	-26.2	-1106.4	12.0
GreenCanyon	5911A16	Genesis	87.74	4.36	NaN	3.16	NaN	0.64	1.48	0.58	0.55	0.99	-220.6	-32.7	-1152.1	-29.0	-1124.5	-29.6	-1121.5	-27.3	-1118.0	-27.9	-1113.8	-26.1	-1107.2	11.7

GreenCanyon	59099A7(RepeatSample)	Genesis	89.31	4.31	NaN	3.18	NaN	0.58	1.19	0.37	0.31	0.34	-222.4	-322.7	-1511.8	-29.0	-1124.6	-29.6	-1113.1	-27.3	-1160.0	-27.9	-1133.3	-26.2	-1108.3	11.9
GreenCanyon	59099A12ST4	Genesis	84.41	5.90	NaN	4.41	NaN	0.86	1.87	0.66	0.60	0.89	-19.9	-333.3	-1581.2	-29.6	-1128.0	-30.0	-1122.5	-27.7	-1120.4	-28.2	-1133.9	-26.7	-1109.1	8.2
GreenCanyon	59099A3	Genesis	87.59	4.72	NaN	3.18	NaN	0.62	1.39	0.51	0.49	0.89	-9.3	-325.5	-1449.2	-28.8	-1124.0	-29.5	-1121.2	-27.3	-1117.6	-27.6	-1111.8	-26.4	-1109.0	11.1
Gre	799	Gen	88.	5.	NaN	3.	NaN	0.	1.	0.	0.	0.	-12	-31	-14	-28	-12	-29	-11	-26	-11	-27	-11	-26	-10	10.2

enCanyon	6A5	esis	26	41		28		59	09	31	27	28	.4	.8	6.2	.3	3.5	.0	8.0	.9	5.4	.3	0.5	.1	8.7	
GreenCanyon	5911A2BP1	Genesis	85.26	6.14	NaN	3.85	NaN	0.73	1.49	0.52	0.50	0.96	-10.9	-31.9	-1150.4	-28.4	-1122.3	-29.1	-1188.3	-26.9	-1188.3	-27.4	-110.2	-26.4	-1109.0	8.5
GreenCanyon	7996A4	Genesis	90.44	3.46	NaN	2.31	NaN	0.51	1.08	0.45	0.45	0.90	-13.8	-31.8	-1441.1	-28.2	-1120.3	-29.1	-1121.1	-26.9	-1116.3	-27.4	-1111.8	-26.2	-1110.2	15.7
GreenCanyon	5911A1ST3	Genesis	87.00	5.94	NaN	3.61	NaN	0.64	1.20	0.36	0.30	0.34	-13.0	-32.1	-1449.1	-28.4	-1122.1	-29.1	-1119.6	-26.9	-1116.8	-27.4	-1110.2	-26.0	-1106.5	9.1
Gre	590	Gen	84.	7.	NaN	4.	NaN	0.	1.	0.	0.	0.	-17	-31	-15	-28	-12	-28	-12	-26	-11	-27	-10	-25	-10	7.1

enCanyon	9A15ST1	esis	37	52		33		75	39	39	35	38	.0	.6	0.0	.0	2.7	.8	0.0	.6	6.0	.1	9.3	.9	7.3	
SigsbySubBasin	HA2-sidetrack	Diana-Hoover	91.66	3.63	NaN	2.51	NaN	0.47	0.39	0.11	0.07	0.09	NaN	-31.5	-126.1	-27.25	-112.2	NaN	NaN	NaN	NaN	NaN	NaN	NaN	NaN	14.9
SigsbySubBasin	HA5-sidetrack	Diana-Hoover	89.18	4.11	NaN	2.65	NaN	0.41	0.36	0.08	0.05	0.05	NaN	-31.7	-132.2	-27.54	-113.8	NaN	NaN	NaN	NaN	NaN	NaN	NaN	NaN	13.2
SigsbySubBasin	SD1	Diana-Hoover	91.91	3.82	NaN	2.04	NaN	0.49	0.62	0.26	0.15	0.31	NaN	-28.8	-122.6	-26.56	-116.0	NaN	NaN	NaN	NaN	NaN	NaN	NaN	NaN	15.7

Sigsby Sub Basin	DB2-ST4	Diana-Hoover	91.34	3.46	NaN	1.88	NaN	0.47	0.61	0.26	0.21	0.74	NaN	-28.9	NaN	-26.5	NaN	-26.0	NaN	-27.3	NaN	-26.0	NaN	-23.8	NaN	17.1
Sigsby Sub Basin	DB-2 Diana Hoover 75° C extraction	Diana-Hoover	91.34	3.46	NaN	1.88	NaN	0.47	0.61	0.26	0.21	0.74	NaN	-28.9	NaN	-26.5	NaN	-26.0	NaN	-27.3	NaN	-26.0	NaN	-23.8	NaN	17.1
Sigsby Su	HA-1QAY-	Diana-Hoo	90.54	4.78	NaN	3.09	NaN	0.52	0.48	0.10	0.06	0.06	NaN	-30.7	-1129.7	-27.31	-1115.7	NaN	NaN	NaN	NaN	NaN	NaN	NaN	NaN	11.5

bBasin	710	ver																						
SigsbySubBasin	Madison(MP-1)	Diana-Hoover	88.86	4.77	NaN	3.83	NaN	0.86	0.80	0.24	0.15	0.14	NaN	-30.7	-1127.7	-27.20	-1114.2	NaN	NaN	NaN	NaN	NaN	NaN	NaN	NaN	10.3
KeathleyCanyon	Hadrian-6	Hadrian	72.32	14.75	0.00	7.88	0.00	0.73	1.80	0.38	0.44	0.43	NaN	-400.5	-1160.1	-32.0	-1117.6	-32.0	-1117.9	-29.1	-1105.5	-29.3	-1105.1	-27.7	-97.2	3.2
KeathleyCanyon	Hadrian-2	Hadrian	96.40	1.18	NaN	1.07	NaN	0.14	0.41	0.09	0.02	NaN	NaN	-400.4	NaN	-30.2	NaN	NaN	NaN	NaN	NaN	NaN	NaN	NaN	NaN	42.9

KeathleyCanyon	Hadrian-2	Hadrian	97.99	0.79	NaN	0.47	NaN	0.04	0.16	0.01	0.01	NaN	NaN	-39.7	NaN	-28.8	NaN	NaN	NaN	NaN	NaN	NaN	NaN	NaN	NaN	77.6
WalkerRidge	Julia1102ST1	Julia	45.76	144.34	NaN	20.34	NaN	2.13	7.42	2.13	2.53	3.03	NaN	-46.1	NaN	-36.8	NaN	-33.9	NaN	-32.0	NaN	-30.8	NaN	-30.0	NaN	1.3
WalkerRidge	Julia1102ST1	Julia	39.72	16.64	NaN	20.74	NaN	2.17	8.10	2.48	3.23	4.76	NaN	-45.3	NaN	-35.9	NaN	-33.6	NaN	-31.6	NaN	-30.5	NaN	-29.7	NaN	1.1
WalkerRidge	Julia1102ST1	Julia	49.40	15.88	0.00	18.87	0.00	1.84	5.96	1.52	1.73	1.85	-18.8	-46.0	-2122.1	-36.7	-1129.3	-33.8	-1117.9	-31.9	-1113.9	-30.7	-1104.5	-29.5	-98.8	1.4
Walke	Julia1	Julia	49.	15.	0.00	18.	0.00	1.89	6.24	1.65	1.89	1.93	-15	-46	-2122	-36	-1129	-33	-1118	-31	-1113	-30	-1105	-29	-99	1.5

r Ridge	02ST1		54	08		84							.3	.0	.6	.7	.5	.7	.1	.9	.3	.5	.7	.7	.9		

Table 3-δD and $\delta^{13}C$ of Genesis Oil Samples

Well	$\delta^{13}C$	δD
A3 Neb 1	-27.0	-103
A12 ST4 14500	-27.2	-100
A7 14200	-27.2	-102
A15 ST1 Neb 3 Upper	-27.0	-101
A4 Neb 3 Lower	-27.0	-101

Declaration of interests

☒ The authors declare that they have no known competing financial interests or personal relationships that could have appeared to influence the work reported in this paper.

☐The authors declare the following financial interests/personal relationships which may be considered as potential competing interests: